Contrib Mineral Petrol (2010) 159:839–862
DOI 10.1007/s00410-009-0458-6

ORIGINAL PAPER

Geochemical investigation of a semi-continuous extrusive basaltic section from the Deccan Volcanic Province, India: implications for the mantle and magma chamber processes

Kopparapu Vijaya Kumar · Chakradhar Chavan · Sariput Sawant · K. Naga Raju · Prachiti Kanakdande · Sangita Patode · Krishna Deshpande · S. K. G. Krishnamacharyulu · T. Vaideswaran · V. Balaram

Received: 6 April 2009 / Accepted: 22 October 2009 / Published online: 12 November 2009
© Springer-Verlag 2009

Abstract Spatial and temporal variations in the geochemistry of an extrusive basaltic section of Deccan traps record progressive changes in mantle melting and crustal filtration and are relevant to understand continental flood basalt (CFB) magmatism. In the present work we have carried out detailed field, petrographic, density and magnetic susceptibility, and geochemical investigations on a small, semi-continuous extrusive section in the eastern Deccan Volcanic Province (DVP) to understand the role of shallow magma chambers in CFB magmatism. Four formations, Ajanta, Chikhli, Buldhana and Karanja crop out in the Gangakhed–Ambajogai area with increasing elevation. Our studies indicate that: (1) the Karanja Formation represents a major magma addition, as indicated by abrupt change in texture, increases in MgO, CaO, Ni, Cr, and Sr, and drastic decreases in Al_2O_3, Na_2O, K_2O, Rb, Ba, REE, bulk-rock density and magnetic susceptibility; (2) assimilation fractional crystallization, crystal-laden magmas, and accessory cumulus phases influence the trace element chemistry of Deccan basalts; (3) the predicted cumulate sequence of olivine gabbro–leucogabbro–oxide-apatite gabbro is supported by the observed layered series in a shallow magma chamber within the DVP; (4) the initial magma was saturated with olivine, plagioclase, and augite, and final the pressure of equilibration for the Gangakhed–Ambajogai section basalts is $\sim$2 kbar ($\sim$6 km depth); (5) petrophysical parameters act as proxies for magmatic processes; (6) a small layer of oxide-rich basalts may represent the latest erupted pulse in a given magmatic cycle in the DVP; (7) parental basalts to some of the red boles, considered as formation boundaries, might represent small degree partial melts of the mantle; (8) SW Deccan basaltic-types continue into the eastern DVP; and (9) in addition to the magma chamber processes, dynamic melting of the mantle may have controlled DVP geochemistry. The present study underscores the importance of mapping specific stratigraphic intervals in limited areas to understand mantle and magma chamber processes relevant to CFB magmatism.

Keywords Continental flood basalts · Deccan · Petrography · Petrophysics · Geochemistry · Dynamic melting · Magma chambers

Communicated by T.L. Grove.

K. Vijaya Kumar (✉)
Department of Geological and Environmental Sciences, Stanford University, Stanford, CA 94305-2215, USA
e-mail: vijay_kumar92@hotmail.com

K. Vijaya Kumar · S. Patode · K. Deshpande · S. K. G. Krishnamacharyulu
School of Earth Sciences, SRTM University, Nanded 431606, Maharashtra, India

C. Chavan · S. Sawant · K. Naga Raju · P. Kanakdande · V. Balaram
Geochemistry Division, NGRI, Hyderabad 500007, Andhra Pradesh, India

T. Vaideswaran
Op. Andhra Pradesh, Geological Survey of India, Southern Region, Bandlaguda, Hyderabad 500068, Andhra Pradesh, India

Introduction to processes controlling erupted basalt compositions in continental flood basalt provinces

Most erupted basaltic lavas in continental flood basalt (CFB) provinces do not represent mantle-derived primary melt compositions, but are end products of complex magma chamber processes (Cox 1980; Farnetani et al.

1996; O'Hara 2000). Experimental evidence suggests that the depth of melting in CFB provinces could be as deep as 70–100 km (Herzberg and O'Hara 1998); for this pressure range, the primary liquids are picritic (see notes 39–45 in O'Hara 2000). Although minor picritic lavas occur in flood basalt provinces (Gibson et al. 2000 and references therein), most of the basalts are quartz tholeiites with fairly constant MgO contents (5–8 wt.%; Farnetani et al. 1996). The geochemical hiatus between the predicted picritic composition and observed tholeiitic composition is interpreted mainly in terms of polybaric crystal fractionation (e.g., Fram and Lesher 1997; Sen 2001). Although crystal fractionation occurs chiefly at the crust–mantle boundary (Cox 1980), which acts as a density and rheological barrier for high-Mg melts (Sparks et al. 1980; Stolper and Walker 1980) gabbroic fractionation at shallower depths has equal importance in controlling the erupted bulk-rock compositions (Cox and Devey 1987). In addition to polybaric crystallization, variation in the CFB chemistry is attributed to mantle source heterogeneity (e.g., Hawkesworth et al. 1988; Ellam and Cox 1991; Ellam et al. 1992) and to various melting processes (Fodor 1987).

Magma chamber processes and shallow magma dynamics in CFB provinces have an important bearing on evolution of the continental crust. During the growth of magma chambers, continuous replenishment of hot picritic primary melts, continuous fractionation of cumulates, and expulsion of evolved and possibly contaminated basaltic liquids takes place (O'Hara 1977; O'Hara and Mathews 1981; O'Hara and Herzberg 2002). In such a scenario, the geochemistry of erupted basalts only indirectly reflects partial melting processes and source compositions. Complications during crustal filtration, including the chemical effects of plagioclase buoyancy within magma chambers (Elthon 1984), must be considered in interpreting the chemistry of the erupted basalts. It has been argued that uniform MgO contents but variable incompatible elemental ratios of erupted evolved basalts are due to RTF (recharge, tapping and fractionation) processes within the magma chambers (O'Hara and Herzberg 2002), although temporal variations in source compositions within the melting regime and crustal assimilation cannot be discounted.

High-resolution sampling studies in a single continuously exposed lava column within the continental flood basalt provinces are very few (e.g., Philpotts 1998) but have contributed significantly to our understanding of igneous processes (Philpotts et al. 1998, 1999; Philpotts and Dickson 2000, 2002; Boudreau and Philpotts 2002; Jerram et al. 2003). The spatio-temporal variations recorded in the lava column allow us to decipher important information regarding mantle source composition and melting conditions, as well as magma chamber processes.

Geochemistry of Deccan basalts: present understanding

The Deccan traps were erupted predominantly on the Archean crust of the Indian shield (Chakrabarti and Basu 2006; Ray et al. 2008). The major eruption is considered to have taken place around 65 ± 1 Ma (see Pande 2002 for a review of Deccan ages). The traps presently cover an area >500,000 km^2, but originally the area might have exceeded 1.5×10^6 km^2 (Wadia 1975). Deccan flood basalt volcanism is clearly associated with extensional tectonics, which appears due to lithospheric stretching and continental rifting (e.g., Sheth 2005a). Causative mechanisms are not known, but the plume hypothesis is still the favorite (Courtillot et al. 2003; Jerram and Widdowson 2005). The western margin of the Deccan Volcanic Province (DVP) is considered to be a major locus of eruptive centers (e.g., Raja Rao et al. 1978; Beane et al. 1986). The thickness of the traps decreases from west (>3000 m) to east (<100 m), controlled by location of eruptive centers and pre-Deccan topography (Mahoney et al. 2000; Jay and Widdowson 2008).

A comprehensive stratigraphic framework for the Deccan basalts was provided by Beane et al. (1986) based on studies in the Western Ghats; three major subgroups and 11 formations (Cox and Hawkesworth 1984; Beane et al. 1986; Subbarao and Hooper 1988; Subbarao et al. 1988; Lightfoot et al. 1990) have been identified. The maximum combined thickness of the SW Deccan basalts exceeds 3 km (Jay and Widdowson 2008), and they exhibit a southward migration of superposition of formations. Increasing degrees of partial melting from north to south were proposed by Peng and Mahoney (1995), resulting in the decrease in average bulk-rock Nb/Zr, Nb/Y and Ba/Ti. Progressive lithosphere thinning can account for shallower and higher degrees of melting in the southern parts of the DVP (Kumar 2003). Krishnamurthy et al. (2000) suggested a decrease in the incidence of high-Mg basalts with time during the Deccan volcanism.

Most of the Deccan tholeiitic basalts (5–8 wt.% MgO), considered to be evolved products (Furuyama et al. 2001) of high-Mg basaltic/picritic primary melts, show mineralogic and major element chemical similarities to mid-ocean ridge basalts, whereas in trace element chemistry they are more similar to oceanic island basalts (Melluso et al. 2006). Crustal filtering both at high and low pressures played an important role in controlling the chemistry of erupted Deccan basalts (Agarwal et al. 1990; Aoki et al. 1992; Furuyama et al. 2001; Sano et al. 2001). The importance of crystal settling in the evolution of Deccan basalts has been emphasized by Cox and Mitchell (1988). They suggested that only denser Deccan liquids are porphyritic, with phenocrysts being strongly biased towards plagioclase; in contrast, almost all the crystals were removed from the less

dense aphyric melts. In the porphyritic rocks, most of the olivine and pyroxene may have been removed by crystal settling, fractionation being induced by density differences between crystals and liquid. Cox and Devey (1987) suggested that a parental magma with 7% MgO may crystallize 50% gabbroic cumulates to generate residual liquids with 5% MgO. Because plagioclase is only 50% of the fractionating mineralogy, diagnostic chemical signatures of plagioclase fractionation (especially decrease in Sr) are not readily documented in the Deccan low-Mg basaltic liquids (Cox and Devey 1987). Higgins and Chandrasekharam (2007) speculated on the presence of sub-volcanic magma chambers beneath the Deccan basalts based on their studies of giant-plagioclase basalts (plagioclase megacrysts up to 50 mm long).

Prima facie evidence for crystal fractionation at shallower DVP depths comes from the Phenai Mata layered igneous complex (Sukheswala and Sethna 1969; Prinzhofer et al. 1988). This complex occurs along the NW periphery of the Deccan traps, possibly within a paleorift structure (Koroleva et al. 2002). Cumulate rocks from bottom to top range from troctolitic gabbro to gabbro–leucogabbro (including anorthosite) and oxide-rich gabbro. Further, Bhattacharji et al. (2004) demonstrated the existence of subsurface magma chambers in the Deccan Volcanic Province based on 3-D modeling of gravity data.

The geochemical features of most of the erupted Deccan traps can be explained by mixing models between the least contaminated Ambenali-type mantle-derived magmas and three types of contaminants: (1) granitic upper crust, (2) amphibolitic, granulitic lower crust and (3) continental lithosphere mantle (Mahoney et al. 1982; Cox and Hawkesworth 1984, 1985; Lightfoot and Hawkesworth 1988; Peng et al. 1994; Dessai et al. 2008). The Bushe and Poladpur units show evidence of contamination with upper crustal materials, whereas the Mahabaleshwar Formation shows evidence for lower crustal contamination or contamination by continental lithospheric mantle (Lightfoot and Hawkesworth 1988; Lightfoot et al. 1990). Additionally, assimilation of shale by Deccan basaltic magma was demonstrated by Chandrasekharam et al. (2000). In Deccan, the least fractionated [high Mg # (Mg/Mg + Fe mol. prop.) rocks] appear to be most contaminated, implying that most of the contamination took place during magma ascent or before fractional crystallization within the shallower magma chambers (Devey and Cox 1987; Lightfoot et al. 1990; Mahoney et al. 2000). Fractional crystallization accompanied by assimilation has been demonstrated in only very few cases (Sheth and Melluso 2008). Further, Sheth (2005b) speculated that a part of the Deccan basaltic magmas might have been derived by melting of eclogitized ancient oceanic crust trapped in the Indian continental lithosphere. The geochemistry of erupted Deccan tholeiitic basalts is thus controlled by crystal settling at both deeper and shallower depths and crustal contamination, in addition to the mantle processes (see Chatterjee and Bhattacharji 2008).

Spatial variation in the Deccan basalt chemistry, based on regional-scale analyses and chemostratigraphy correlations, is well understood. Further, many of the intensive studies on the Deccan basalts are centered on the Western Ghats, Kutch, and Narmada-Tapi areas (Najafi et al. 1981; Beane et al. 1986; Subbarao et al. 1994; Peng et al. 1998; Chandrasekharam et al. 1999, 2000; Mahoney et al. 2000; Shukla et al. 2001; Melluso et al. 2004; Sheth et al. 2004, 2009). However, focused studies on the spatio-temporal variations in petrological, geochemical and petrophysical characteristics within a single continuous extrusive section are rare in the eastern DVP (Shrivastava and Pattanayak 2002; Jay and Widdowson 2008 and references therein).

In the present study, we have undertaken a high-resolution chemostratigraphy investigation of a semi-continuous extrusive sequence from the eastern Deccan Volcanic Province in order to evaluate mantle and magma chamber processes. We have focused our study on a 250 m thick eastern DVP transect covering a continuous exposure of erupted basalts. We conducted systematic sampling across four recognizable basalt formations. Forty samples were collected across the 250 m section and 27 samples were analyzed for major, trace and rare earth elements in order to obtain a spatial resolution to identify units representing abrupt chemical changes. Special care was taken to analyze samples across formation boundaries to understand magma chamber processes beneath continental flood basalts. One sample each of a fragmentary top and a red bole were also analyzed to understand their relationship with associated unaltered basalts. Additionally, we also measured bulk-rock density and magnetic susceptibility on minicores from representative samples to understand their relationship to the geochemistry.

Geologic setting, field relations and sampling

Several of the SW Deccan formations extend into the SE and eastern Deccan, particularly the Ambenali and Poladpur formations (e.g., Mitchell and Widdowson 1991; Bilgrami 1999). The SE and eastern Deccan Volcanic Province has been recently mapped in detail by Jay and Widdowson (2008), who suggested that the Ambenali and Poladpur chemo-types dominate the area. The present study area falls in a narrow window that has not been chemostratigraphically mapped hitherto. The sampled continuous transect falls between the towns of Gangakhed and Ambajogai (the G–A section) (Osmanabad Quadrangle of Geological Survey of India and covers a part of Survey of India Topo

sheets 56B/5, 56B/6 and 56B/9) within the eastern Deccan Volcanic Province (Fig. 1). Although, thickness of some of the formations is relatively less and could be designated as lava-packages, we have adopted the formational terminology introduced by Geological Survey of India to avoid confusion. From north to south, a gradual increase in elevation of 250 m (between 400 and 650 m elevated terrain above mean sea level) is recorded over a horizontal distance of 45 km. The area was mapped to understand geologic relations, identify different marker zones, and document the stratigraphy of the basalts. Most of the sampling in the present study was carried out along road cuts and quarries. Excellent vertical exposure allowed us to collect samples from identifiable flow units. Care was taken to collect unaltered samples at key locations (for example above and below the red boles) interspersed along the ca 45 km of road traverse. The location and elevation of each sample were recorded employing topographic maps and an altimeter. Flow characteristics and relations with associated flows were recorded for each sample.

We mainly used boles of different colors (khakhi, green, red) and other field features including the type of flow (aa, pahoehoe), presence and absence of vesicles, fragmentary tops and bottom of the aa flows, jointing patterns, percentage of phenocrysts, etc. as marker horizons and guides to distinguish individual flows of a formation and the formational contacts. Although the field and petrographic criteria used in this study to distinguish different formational boundaries is not unique and fraught with uncertainties, geochemical distinctions among the four formations (see later sections) validate our approach.

Four formations, namely the Ajanta, Chikhli, Buldhana and Karanja, from lower to higher elevation (stratigraphic horizon) respectively, are exposed. In the studied section, the Ajanta Formation, forming the base of the stratigraphic column, is the only pahoehoe flow with characteristic reddish brown ropy surface structure. This flow is amygdaloidal with amygdales ranging from few mm to $\sim$2 cm filled with secondary minerals including calcite, zeolites and chalcedony. Pipe vesicles are common and range in length up to 1–2 cm. Due to its highly vesicular nature, the Ajanta Formation is the most intensely weathered of the mapped formations. Characteristics of compound flows such as massive, poorly jointed and amygdaloidal nature are exhibited by Ajanta basalt. The Chikhli Formation is a single massive flow of possibly limited extent, because at places Ajanta is directly overlain by the Buldhana Formation. Vertical jointing, horizontal fractures, and spheroidal weathering characterize the Chikhli flow. Rarely, a basal flow breccia of this formation is exposed. The Chikhli basalt is moderate to highly porphyritic with plagioclase size ranging up to 2 cm. The Buldhana Formation is a thick, single massive aa flow. The flow shows columnar joints ranging more than 15–20 m in length and ca 3 m in width. Contacts between the lower three formations are typified by thin red bole layers suggesting that time gaps between the different basaltic extrusions were minimal. The contact between the Buldhana and Karanja formations

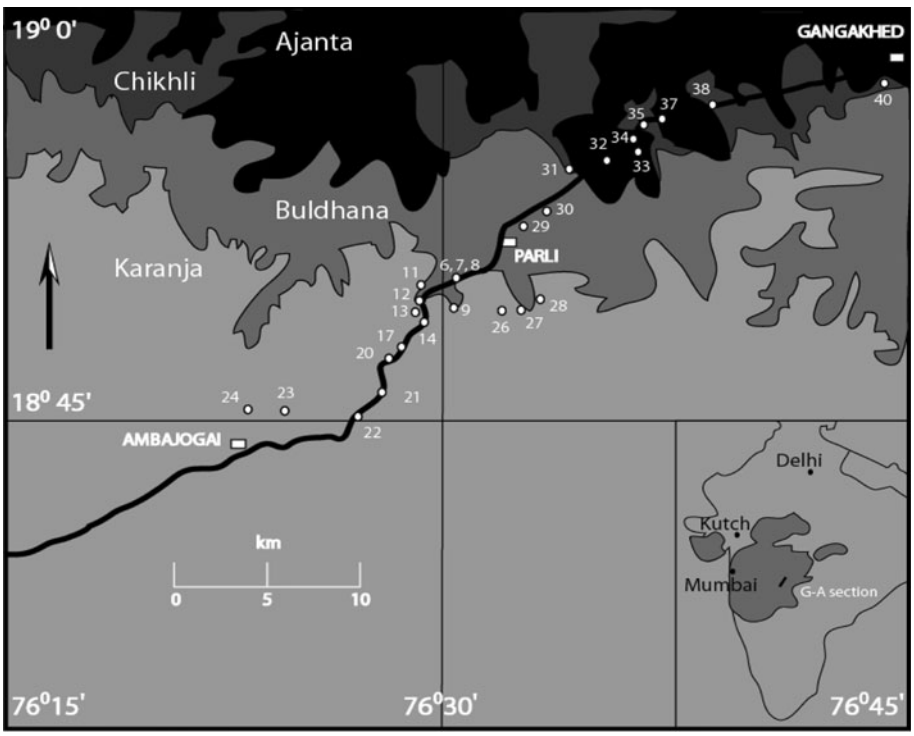

Fig. 1 Geological map of the Gangakhed–Ambajogai (G–A) section of the eastern Deccan Volcanic Province, modified after the GSI quadrangle map of the Osmanabad district, displaying Ajanta (*black*), Chikhli (*dark grey*), Buldhana (*lighter grey*) and Karanja (*very light* grey) formations. The elevation gradually increases from north to south in the mapped area. Locations of the geochemically analyzed samples are indicated. Inset shows outline map of part of India with location of G–A section within the Deccan Volcanic Province (shown in *darker grey shade*)

is exposed in the form of a very thick red bole with a maximum thickness of ca 3 m. The latter is highly friable with variable thickness, apparently following the local topography. Buldhana basalts are moderately porphyritic. The lower six flows of the total 26 Karanja flows are mapped in the present study. The fragmentary top of the lowermost flow of the Karanja Formation (K1 flow) contains broken angular fragments of basalts having different sizes and shapes in the basaltic matrix. The second Karanja flow (K2 flow) contains a complete spectrum of columnar structures including a lower colonnade followed by a middle entamblature zone and an upper colonnade. The middle, massive part contains columnar joints 3 m high and 0.3–0.6 m wide; splay joints are developed in the colonnade zone. A thick red bole is developed between the second and third flows of the Karanja Formation. A capping red bole 1–2 m thick with undulating structure is baked and locally turned into green/khaki color. Chilled basalt is present just above the red bole, but has undergone extensive weathering. Pyroclastic material is present just below the fragmentary bottom of the fourth flow. The fifth flow is a simple aa flow with a fragmentary top. The sixth flow of the Karanja Formation shows squeeze-up structure, possibly formed by quenching of the lava. The squeeze-ups are present as easily recognizable blocks between the massive basalts. This flow shows characters of compound flow. Karanja basalts are sparsely to moderately porphyritic. Based upon all these field observations we have determined the stratigraphy for basalts in the Gangakhed–Ambajogai section of the eastern DVP (Fig. 2). As the flows are near horizontal, we have used elevation above sea levels as proxy for stratigraphic horizons.

Petrography

Basalts of the four formations of the G–A section are essentially composed of plagioclase and clinopyroxene with variable proportions of devitrified glass and oxide minerals. The G–A section basalts display porphyritic,

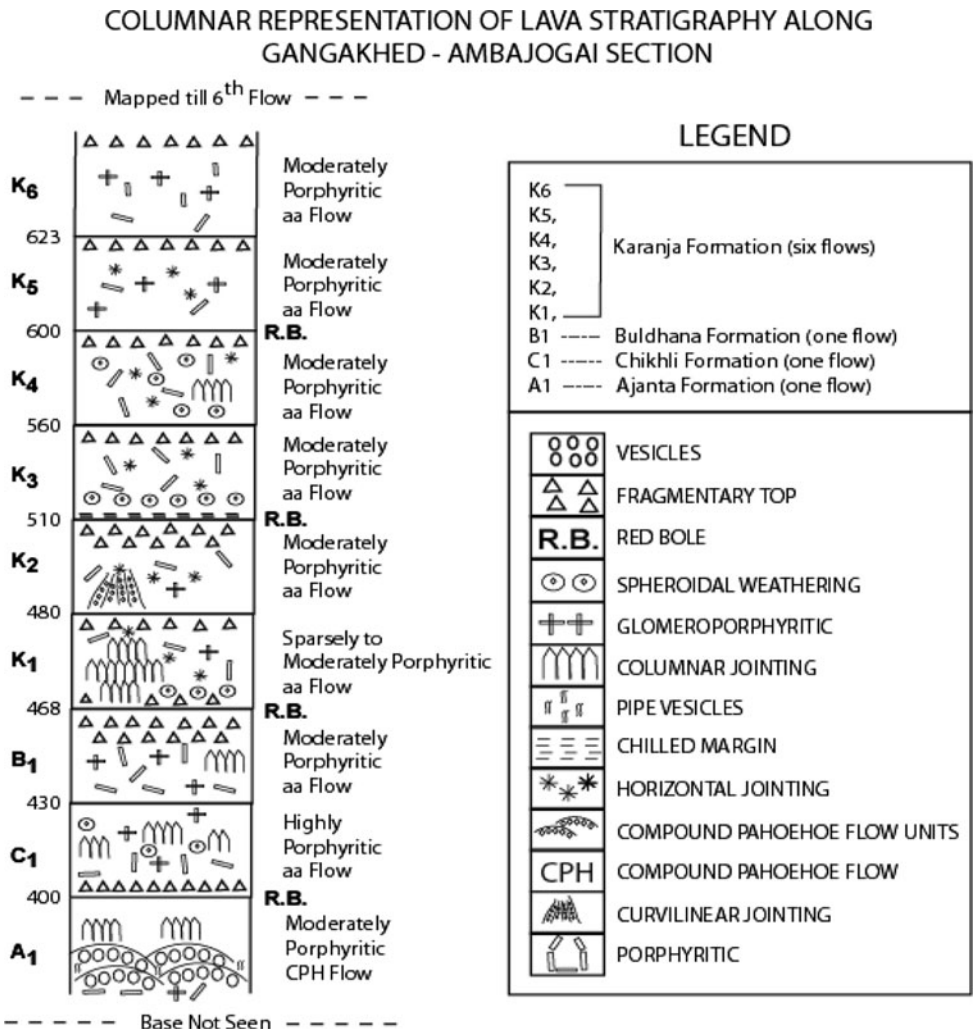

Fig. 2 Stratigraphic column for the lava stratigraphy along the G–A section, eastern DVP. Elevations shown on left of the column are in meters above mean sea level. Flow characteristics are shown on the *right side* of the column

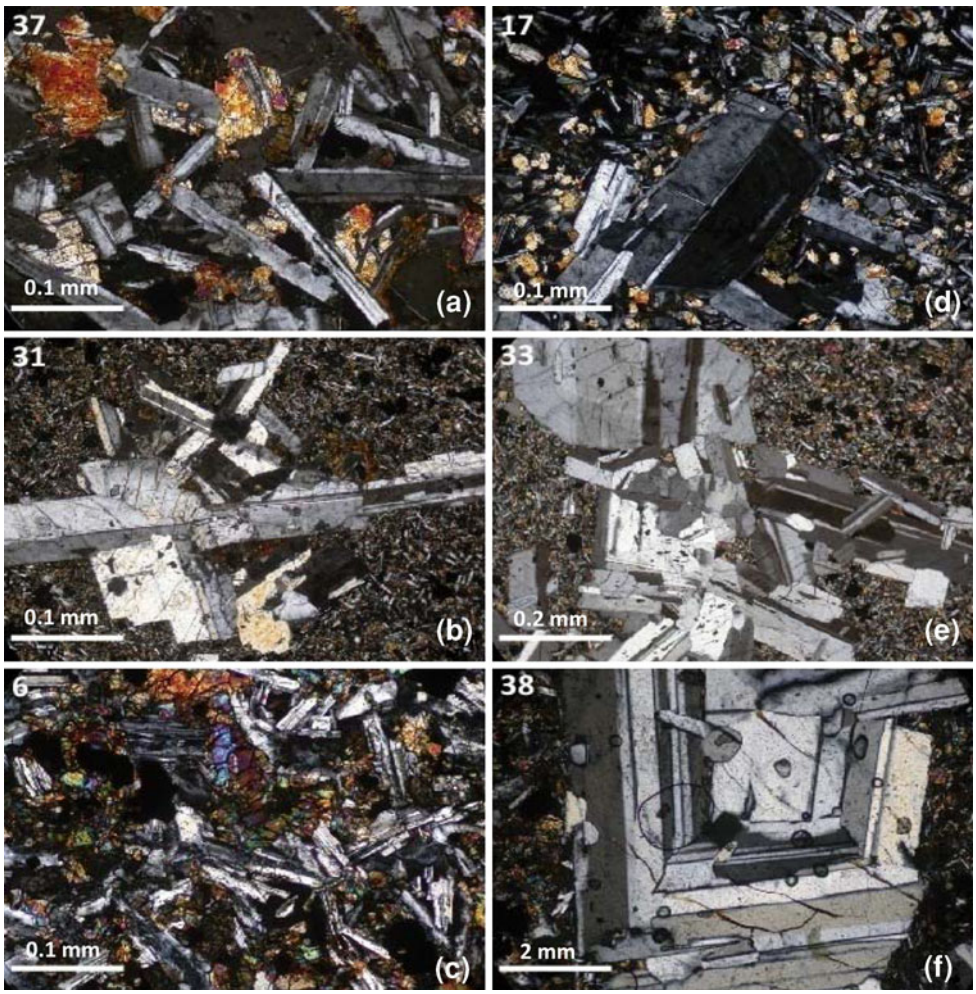

Fig. 3 Photomicrographs depicting textural features and mineral associations in the G–A section basalts. Sample numbers are shown in the *upper left corner* of each picture. (**a**) Basalt from the Ajanta Formation displaying subophitic to intergranular texture; (**b**) glomeroporphyritic texture in Chikhli basalts; note very fine groundmass; (**c**) oxide- and pyroxene-rich basalt exhibiting intergranular texture in Buldhana basalts; (**d**) porphyritic texture in evolved Karanja basalt; (**e**) zoned and resorbed phenocrystic plagioclases from the Chikhli basalts; (**f**) Chikhli Formation is similar to giant plagioclase basalts reported from other parts of the Deccan Volcanic Province (Higgins and Chandrasekharam 2007)

glomeroporphyritic, seriate, vitriophyric, intergranular and subophitic textures (Fig. 3a–d). Rare specks of orthopyroxene are present only in the Buldhana Formation. Microphenocrysts of olivine and clinopyroxene are restricted to the lower flows of the Karanja Formation. Ajanta, Chikhli, Buldhana and evolved Karanja basalts contain abundant plagioclase phenocrysts. Modal plagioclase is highest in the Chikhli unit, and pyroxene + oxide proportions are highest in the Buldhana basalts. At places, segregations of plagioclase phenocrysts define a glomeroporphyritic texture, especially in the Chikhli basalts (Fig. 3e). Phenocrystic plagioclase shows conspicuous zoning (Fig. 3f) in the basalts of Chikhli, Buldhana and also in the stratigraphically higher Karanja basalts. Some of the basalts contain resorbed plagioclase phenocrysts. The percentage of opaque minerals exhibits a continuous increasing trend from Ajanta through Chikhli to Buldhana formations, and the proportion of devitrified glass is much higher in the Karanja basalts. In some rocks, plagioclase shows a gradation in grain size from the coarse phenocrysts to the fine-grained groundmass. Proportions of plagioclase and pyroxene within the groundmass are variable; only in a few basalts pyroxene is more abundant than plagioclase. Locally, pyroxene is altered to reddish-brown biotite. Groundmass plagioclase laths swirl around phenocrystic plagioclases, denoting magma flowage, which is further supported by oriented plagioclase phenocrysts in some of the porphyritic basalts. In the groundmass, alternate microzones rich in clinopyroxene and plagioclase define mottled texture similar to the ones reported from Holyoke flood basalt (Philpotts et al. 1998). The grain size of groundmass minerals has a wide range from very fine-grained (<0.01 mm) to up to mm dimensions. Based on textural features, the sequence of crystallization in the G–A basaltic liquid was (olivine) → plagioclase → clinopyroxene → orthopyroxene → oxides → apatite.

Whole-rock geochemistry

All the samples were powdered to ~75 μm size by a "HERZOG" swing-grinding mill using a hard chrome steel grinding tool. For analysis of the major elements, sample pellets were prepared by pressing the rock powder with a

backing of boric acid powder in collapsible aluminum cups at 20 tons of pressure employing a "HERZOG" hydraulic press model TP2d to give pellets 40 mm in diameter. A Philips PW 1400 microprocessor controlled, sequential wavelength dispersive X-ray flourescence spectrometer with 100 KVA X-ray generator and 72 position automatic sample changer to load and unload the samples was employed to measure different peaks and background counts for the major elements. Samples were calibrated using JGb1. Total Fe was measured as Fe_2O_3. Analytical uncertainty was around 1% for Al_2O_3, MgO, Fe_2O_3, CaO, Na_2O, K_2O and 2% for SiO_2 and P_2O_5.

Standard acid dissolution techniques were employed for dissolving 50 mg of sample for the estimation of trace elements by ICP-MS (VG-Plasmaquad). Elements were converted into ions in the inductively coupled plasma and the ions, based on their mass, were counted by a Quadruple Mass Spectrometer (with counts directly proportional to the concentration of the elements). To determine the accuracy and precision of the instrument, replicate analysis of the standards and a basaltic sample were carried out. Based on these measurements, the precision of our analysis is better than 5% of the amount present. Whole-rock geochemistry of the G–A section basalts is given in Table 1.

On the basis of norms, all analyzed G–A section basalts are quartz tholeiites with variable proportions of normative hypersthene. Based on the major element composition and normative mineralogy, the G–A section basalts are classified as low-K subalkaline quartz tholeiites. They exhibit iron enrichment trends characteristic of tholeiitic basalts.

Liquid-lines-of-descent in terms of major and trace elements are discussed assuming that the parental liquid to all the G–A section basalts was similar to the least-differentiated Karanja basalt (Table 1, sample 26 with MgO = 6.35 wt.%). The compositions were corrected for phenocrysts and corrected compositions are presented in Harker-type variation diagrams using MgO as an index of differentiation (Fig. 4). We have depicted the liquid-lines-of-descent based on variations in Al_2O_3, CaO, Sr and Cr contents as they critically record fractionation processes in a basaltic magma. Fractionation of plagioclase and clinopyroxene in the G–A section basalts is reflected by continuous decrease in Al_2O_3, CaO, Sr and Cr with decreasing MgO contents. The amount of decrease in Ni (40 ppm) for a decrease of 2% MgO (Table 1) indicates that olivine is not a major fractionating phase. The fractionation paths of G–A section basalts mimic the liquid-lines-of-descent exhibited by experimentally constrained Deccan basaltic melts (Sano et al. 2001) and calculated gabbro fractionation (Fig. 4).

The G–A section basalts show moderately fractionated rare earth element (REE) patterns with small to moderate negative europium anomalies (Fig. 4e). From the Ajanta to Buldhana formations, there is a gradual increase in absolute abundances and magnitude of negative Eu anomalies (Fig. 4e). Karanja basalts show much lower abundances (except for an altered sample; Table 1 and Fig. 4e), and the chondrite-normalized REE patterns of the Karanja Formation show slightly LREE depletion [$(La/Nd)_N < 1$; Fig. 4e)] and fractionated HREE patterns; these are quite distinct from those of the Ajanta, Chikhli and Buldhana formations which have LREE enriched ($La/Nd_N > 1$) and fractionated HREE. The presence of small amounts of cumulus plagioclase may have slightly decreased the absolute REE abundances in the Chikhli basalts. Note the crossing of REE patterns, especially in the HREE segment.

In the NMORB-normalized incompatible element diagram (Fig. 4f) the analyzed basalts show fractionation of incompatible elements from left to right with negative spikes for K and positive spikes for Pb and Ti characteristic of oceanic island basalt (see Sun and McDonough 1989). Much lower enrichment of highly incompatible elements (even at comparable MgO contents; Table 1) and pronounced troughs for Rb in the Karanja basalts are evident. Simple crystal fractionation cannot reproduce the level of enrichment in incompatible elements (by an order of magnitude; Fig. 4f) for a 2% variation in MgO (Table 1) in the G–A section basalts; inputs from continental crust seem to be necessary as discussed in later sections.

The fragmentary top exhibits geochemical traits of both Buldhana and Karanja formations (Table 1; Fig. 4e). It shows LREE depletion in chondrite-normalized REE pattern similar to the Karanja basalts but with much higher absolute concentrations akin to Buldhana basalts (Fig. 4e). Red bole seems to have gained Fe_2O_3, K_2O, and mobilized (lost) SiO_2, Na_2O, Al_2O_3 and P_2O_5. Apatite and the albitic component of plagioclase seem to have been affected by weathering. Na_2O is near zero in red bole, suggesting that the albitic component has been completely eliminated from the parental rock. Elements that could adsorb onto clay surfaces (i.e., large ion lithophile elements) are all enriched in the red bole. Red bole shows a "positive Ce" anomaly and a more fractionated pattern than those of basalts (Fig. 4g). The geochemical traits of red bole do not match either the Buldhana or Karanja basalts. If the red bole was indeed derived by weathering of a parental material other than the associated basalts, then assessment on the mobility of elements based on comparison with underlain unaltered basalt would lead to erroneous conclusions.

Table 1 Representative whole-rock major and trace element composition, and petrophysics of the G–A section basalts, eastern Deccan Volcanic Province, India

	Ajanta			Chikhli					Buldhana				
Sample no.	32	34	37	31	33	35	38	40	6	7	8	29	30
Elevation (m)	400	395	398	415	402	408	400	400	460	455	465	435	440
Major elements (wt.%)													
SiO_2	49.91	49.51	49.51	50.18	50.11	50.52	49.98	50.68	49.17	50.37		48.84	49.47
TiO_2	2.35	2.44	2.18	2.34	2.31	2.31	2.39	2.20	3.29	3.20		2.62	3.13
Al_2O_3	12.66	13.13	13.4	13.53	13.13	13.56	13.78	13.16	12.14	12.35		13.27	12.87
$Fe_2O_3^a$	14.53	14.94	14.48	14.94	14.7	14.61	14.55	14.52	16.29	15.95		14.79	16.00
MnO	0.2	0.18	0.18	0.18	0.18	0.18	0.17	0.17	0.2	0.18		0.19	0.20
MgO	5.91	5.41	5.47	4.69	4.61	4.55	4.59	5.29	4.68	4.71		5.09	4.4
CaO	10.36	10.09	10.8	10.11	10.99	10.04	9.99	9.83	8.97	9.01		10.77	9.16
Na_2O	1.87	1.97	2.32	2.44	2.4	2.47	2.53	2.35	2.42	2.49		2.29	2.41
K_2O	0.35	0.26	0.32	0.30	0.32	0.35	0.35	0.47	0.64	0.70		0.21	0.49
P_2O_5	0.33	0.32	0.33	0.25	0.24	0.25	0.26	0.26	0.40	0.43		0.27	0.40
LOI	2.93	1.59	2.12	1.65	1.91	2.76	1.5	1.42	1.53	1.12		2.22	1.83
Total	101.40	99.84	101.11	100.61	100.9	101.6	100.09	100.35	99.73	100.51		100.56	100.36
LFSE (ppm)													
Cs	0.20	0.07	0.12	0.22	0.20	0.16	0.13	0.12	0.24	0.39	0.65	0.25	0.29
Rb	8.90	4.50	5.53	8.12	7.98	6.94	5.56	7.94	18.7	21.9	23.9	14.2	11.9
Ba	111	82	104	116	117	117	122	134	153	147	134	144	136
Sr	243	240	239	249	240	245	251	249	217	215	207	201	205
HFSE (ppm)													
Th	1.60	1.60	4.60	1.59	1.56	1.56	1.62	1.63	2.41	2.26	2.27	2.50	2.43
U	0.36	0.36	0.39	0.34	0.36	0.36	0.38	0.38	0.61	0.56	0.56	0.64	0.56
Nb	11.2	11.9	12.0	11.3	11.2	11.4	11.6	11.5	18.4	18.5	17.6	18.1	17.5
Ta	2.23	2.64	3.96	2.22	2.26	2.37	2.39	2.36	3.78	3.44	3.30	3.71	3.43
Pb	4.72	7.14	2.56	6.91	4.33	4.87	4.69	5.62	7.92	6.93	6.44	4.85	6.24
Zr	163	159	171	169	164	164	170	172	249	249	248	246	244
Hf	3.64	3.74	0.43	3.88	3.77	3.65	3.85	3.95	5.39	5.09	5.12	5.41	5.42
Y	32.6	32.6	34.0	33.1	32.1	32.8	33.5	33.3	48.6	46.8	46.6	47.2	46.8
REE (ppm)													
La	12.7	12.6	13.2	12.6	12.2	12.1	12.3	12.8	17.9	17.8	17.3	17.8	17.2
Ce	31.4	31.2	33.0	30.6	30.4	30.2	31.4	31.1	44.6	43.7	42.6	44.1	43.7
Pr													
Nd	21.2	22.0	23.1	22.0	21.5	21.7	21.7	22.1	31.2	30.2	30.3	31.7	30.4
Pm													
Sm	5.65	5.68	5.95	5.65	5.54	5.64	5.62	5.74	7.61	7.47	7.6	7.74	7.71

Table 1 continued

	Ajanta			Chikhli					Buldhana					
Sample no.	32	34	37	31	33	35	38	40	6	7	8	29	30	
Elevation (m)	400	395	398	415	402	408	400	400	460	455	465	435	440	
Eu	1.78	1.75	1.85	1.78	1.80	1.77	1.83	1.84	2.28	2.25	2.231	2.32	2.31	
Gd	6.82	6.86	7.22	6.88	6.86	6.74	7.00	7.21	9.79	9.21	9.15	9.64	9.52	
Tb														
Dy	5.50	5.57	5.92	5.69	5.59	5.58	5.70	5.88	7.89	7.48	7.576	8.00	7.87	
Ho	1.11	1.13	1.19	1.13	1.13	1.10	1.14	1.15	1.59	1.51	1.524	1.61	1.62	
Er	3.18	3.22	3.45	3.28	3.31	3.22	3.36	3.28	4.70	4.35	4.427	4.72	4.70	
Tm														
Yb	2.60	2.63	2.73	2.54	2.64	2.59	2.60	2.68	3.78	3.60	3.627	3.83	3.84	
Lu	0.39	0.39	0.43	0.40	0.39	0.39	0.39	0.40	0.59	0.54	0.562	0.59	0.59	
Transition metals (ppm)														
Cr	90.7	84.3	91.8	75.4	68.8	65.0	80.0	73.6	102	101	109	84.3	81.1	
Co	50.3	50.8	51.2	52.8	51.4	52.5	54.4	54.0	54.1	51.3	52.2	51.0	51.5	
Ni	43.8	40.6	42.6	46.3	41.9	40.5	49.2	48.3	48.5	46.3	46.1	45.7	45.9	
Sc	34.4	34.1	34.4	34.2	33.1	33.8	34.3	34.7	38.6	37.6	37.3	35.3	36.1	
V	407	406	400	405	388	390	404	403	474	481	465	450	457	
Cu	203	191	209	208	207	191	209	213	326	342	139	385	298	
Zn	144	142	153	143	141	135	143	153	201	200	196	194	188	
Petrophysics														
Density (g/cm^3)	2.80	2.95	2.90	3.00	3.20	3.00	3.10	3.00	3.15	3.22			3.15	
Magnetic intensity (CGS units)	4118	6516	3929	4256	4334	4502	3922	4798	1422	334			901	
Magnetic susceptibility (CGS units)	2711	2662	2414	1450	2705	2553	2629	2788	3666	3802			3656	
Liquidus T °C	1146	1132	1138	1112	1104	1108	1110	1135	1124	1124			1110	

	Karanja													
Sample no.	9	11[b]	12	13	14	17	20	21	22	23	24	26	27[c]	28
Elevation (m)	470	473	470	475	480	505	555	596	620	638	648	470	468	465
Major elements (wt.%)														
SiO_2	49.04	44.80	50.06	50.09	49.21	49.15	49.65	48.59	49.8	48.13	49.11	48.32	38.39	49.66
TiO_2	2.4	3.30	2.17	2.33	2.36	2.1	2.67	2.65	2.69	2.7	2.62	2.32	1.72	2.29
Al_2O_3	12.67	11.47	13.59	13.14	13.1	13.61	13.24	12.88	12.56	13.23	13.25	13.56	8.02	12.19

Table 1 continued

	Karanja													
Sample no.	9	11[b]	12	13	14	17	20	21	22	23	24	26	27[c]	28
Elevation (m)	470	473	470	475	480	505	555	596	620	638	648	470	468	465
$Fe_2O_3^a$	14.75	15.90	14.46	14.44	14.83	14.13	14.83	15.81	15.55	15.67	14.87	14.24	12.97	14.44
MnO	0.16	0.17	0.18	0.17	0.18	0.18	0.19	0.19	0.17	0.19	0.19	0.17	0.25	0.17
MgO	6.24	6.10	5.09	5.51	5.59	5.7	5.22	5.29	5.51	5.37	5.25	6.35	5.84	6.07
CaO	10.6	7.92	10.62	10.08	10.51	10.9	10.79	10.72	10.22	10.36	10.75	11.44	9.65	10.92
Na_2O	2.16	1.34	2.3	2.27	2.2	2.22	2.34	2.16	2.29	2.14	2.27	2.12	0.02	2.07
K_2O	0.17	0.25	0.25	0.28	0.29	0.25	0.18	0.21	0.32	0.21	0.21	0.15	0.55	0.17
P_2O_5	0.29	0.35	0.17	0.29	0.21	0.17	0.28	0.21	0.35	0.35	0.23	0.32	0.09	0.44
LOI	1.68	8.5	1.43	2.08	1.16	1.69	2.68	2.18	2.29	2.6	2.22	2.31	22.7	2.23
Total	100.16	100.10	100.32	100.68	99.64	100.10	102.07	100.89	101.75	100.95	100.97	101.3	100.20	100.65
LFSE (ppm)														
Cs	0.03	0.10	0.13	0.05	0.19	0.09	0.06	0.11	0.03	0.05	0.11	0.02	0.73	0.02
Rb	1.28	3.89	6.33	3.50	8.80	5.99	3.51	5.35	3.66	2.69	5.41	1.32	21.6	1.19
Ba	77.7	83.1	86.3	92.4	93.0	89.3	84.1	92.3	102	103	85.4	77.6	165	77.6
Sr	242	224	220	218	215	211	210	212	213	219	215	235	266	234
HFSE (ppm)														
Th	0.83	2.35	0.89	0.89	0.95	0.94	0.94	0.98	1.22	1.20	1.04	0.89	1.32	0.90
U	0.21	0.50	0.21	0.21	0.22	0.21	0.24	0.25	0.30	0.28	0.27	0.22	0.19	0.23
Nb	11.4	17.8	10.0	10.0	10.5	8.94	11.8	12.2	15.7	15.5	12.6	10.7	8.36	11.37
Ta	2.13	3.41	1.89	2.00	2.00	1.77	2.23	2.43	3.21	3.20	2.61	2.23	1.62	2.35
Pb	5.75	6.46	6.13	4.77	6.69	6.62	4.81	4.67	4.91	5.53	4.46	4.33	4.46	4.86
Zr	161	248	139	141	149	129	153	162	172	174	164	151	107	161
Hf	3.42	5.23	3.04	3.20	3.24	2.83	3.35	3.61	3.80	3.86	3.72	3.31	2.38	3.62
Y	34.1	41.0	30.7	31.1	32.9	29.3	34.0	34.9	35.1	35.7	35.6	32.7	21.9	34.3
REE (ppm)														
La	8.92	13.6	8.80	8.98	9.52	8.46	9.30	9.70	11.5	11.5	10.0	8.79	7.91	9.14
Ce	23.6	37.4	22.7	23.4	24.3	21.4	24.3	25.5	29.3	29.6	26.2	23.2	31.7	24.6
Pr														
Nd	19.2	27.8	16.9	17.5	18.5	16.5	18.6	19.8	21.5	22.2	20.4	18.6	13.8	19.8
Pm														
Sm	5.22	6.76	4.65	4.78	5.04	4.48	5.10	5.30	5.64	5.74	5.49	5.18	3.38	5.45
Eu	1.74	2.09	1.52	1.55	1.67	1.43	1.68	1.73	1.80	1.81	1.76	1.68	1.18	1.73
Gd	6.49	8.48	5.83	6.02	6.28	5.59	6.69	6.74	6.99	7.11	6.95	6.61	4.00	6.88

Table 1 continued

	Karanja													
Sample no.	9	11[b]	12	13	14	17	20	21	22	23	24	26	27[c]	28
Elevation (m)	470	473	470	475	480	505	555	596	620	638	648	470	468	465
Tb														
Dy	5.53	7.25	4.93	5.07	5.23	4.73	5.59	5.70	6.00	6.02	5.90	5.52	3.67	5.80
Ho	1.10	1.44	1.01	1.03	1.10	0.96	1.10	1.16	1.21	1.21	1.18	1.09	0.76	1.17
Er	3.23	4.13	2.94	2.94	3.16	2.88	3.26	3.37	3.47	3.51	3.54	3.22	2.20	3.43
Tm														
Yb	2.55	3.31	2.31	2.44	2.60	2.28	2.71	2.74	2.80	2.84	2.83	2.57	1.68	2.71
Lu	0.38	0.50	0.36	0.38	0.41	0.36	0.42	0.43	0.42	0.44	0.43	0.39	0.27	0.42
Transition metals (ppm)														
Cr	124	84.5	88.4	69.2	80.0	101	89.4	90.8	100	94.3	104	111	76.7	113
Co	58.2	53.1	56.7	55.9	55.9	56.9	57.5	58.5	55.6	56.7	58.3	55.1	45.4	56.9
Ni	74.2	46.8	53.8	50.6	50.7	52.9	61.8	64.1	60.0	62.0	64.2	71.7	47.7	72.7
Sc	37.4	37.6	37.0	36.7	37.2	36.9	37.9	37.5	35.6	35.9	37.0	34.7	29.3	35.7
V	447	487	406	407	422	392	444	439	422	427	440	416	157	438
Cu	263	301	216	210	234	193	239	256	253	281	259	284	234	241
Zn	168	198	138	140	149	136	168	159	167	162	157	149	87	158
Petrophysics														
Density (g/cm^3)	2.82		3.00	3.00	3.00	2.95	3.00	3.00	2.95	2.98		2.87		2.90
Magnetic intensity (CGS units)	4161		1014	3291	6984	9422	9271	9270	4504	2316		4361		4046
Magnetic susceptibility (CGS units)	1115		1026	2159	1104	1352	1807	1472	1236	1164		1015		2340
Liquidus T °C	1158		1121	1134	1139	1139	1123	1128	1138	1131		1154		1150

[a] Total Fe as Fe_2O_3

[b] Fragmentary top

[c] Red bole

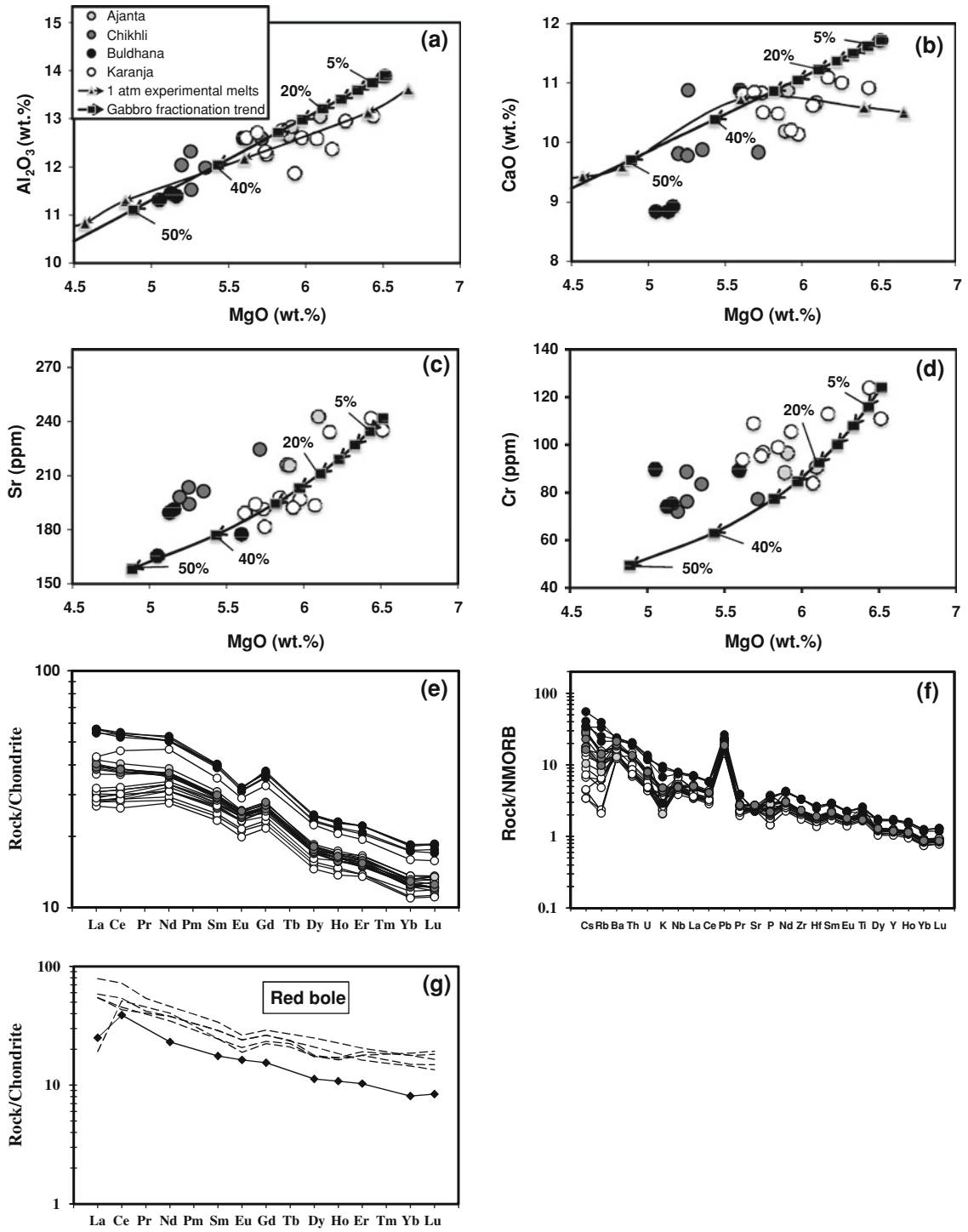

Fig. 4 MgO versus major [(**a**) and (**b**)] and trace [(**c**) and (**d**)] element variations in the G–A section basalts of the eastern DVP. Phenocryst-corrected compositions are plotted in the variation diagrams. Mineral compositions are taken from Sen (1986). The liquid evolution path for 1 atm experimentally produced melts (Sano et al. 2001) and calculated low-pressure gabbro fractionation trend are shown for comparison. The gabbro assemblage considered in the calculations is Pl = 50%, Cpx = 30%, Ol = 2%, Mt = 4%, Ilm = 4%, Ap = 1% and intercumulus liquid (ICL) = 9%. Percentages of fractionation are shown. (**e**) Chondrite-normalized REE patterns for the G–A section basalts. Note the moderately LREE-depleted nature of the Karanja basalts. (**f**) NMORB-normalized minor and trace element diagram for the G–A section basalts. (**g**) Chondrite-normalized REE patterns for red bole from the G–A section. For comparison, REE patterns for red boles from other parts of DVP (Widdowson et al. 1997; Ghosh et al. 2006) are also shown. Note that red boles have more fractionated LREE/HREE than associated basalts. Also note "Ce peaks" in some of the red boles. Chondrite normalizing values are after Hanson (1980); NMORB normalizing values are after Sun and McDonough (1989)

Petrophysics

Bulk-rock density and magnetic susceptibility for selected freshest basalt samples from the G–A section were measured on 2.5 cm minicores using a balance and magnetic susceptibility meter, respectively; the values reported are averages of at least four minicores. The measured bulk-rock densities (Table 1) were corrected for phenocrysts and are considered to represent liquid densities. These corrected densities are plotted in several figures. Density shows an increasing trend (Fig. 5) with decreasing Mg # [(Mg/Mg + Fe^t) × 100]. Buldhana basalts, with petrographic and geochemical evidence for the saturation of oxide minerals, record the highest measured bulk-rock and liquid densities (Table 1; Fig. 5). During fractionation, an increase in FeO^t and TiO_2 contents is reflected in a comparable density increase. Where plagioclase is the dominant fractionating phase, residual liquid density increases, as is faithfully reflected by the analyzed basalts.

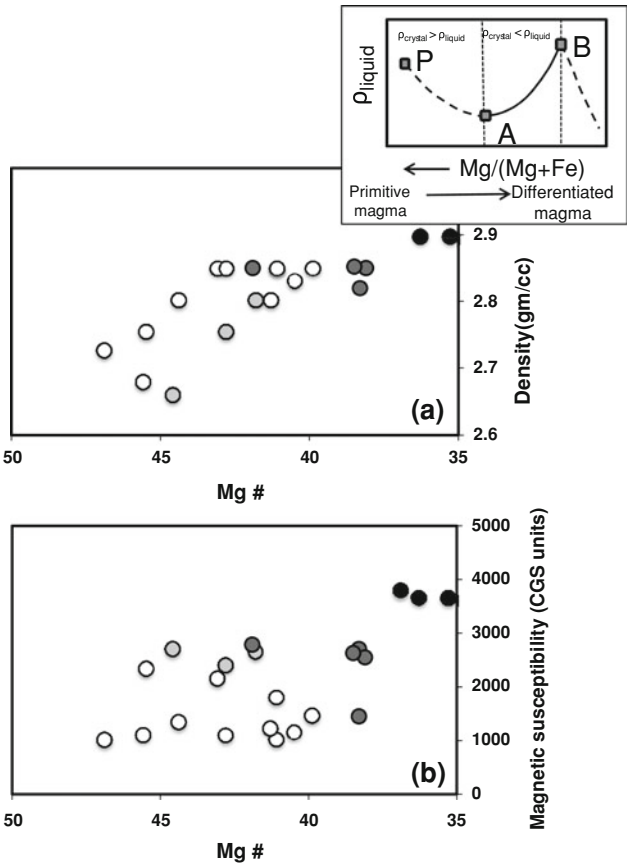

Fig. 5 Mg # [Mg/(Mg + Fe^t) × 100] versus density (**a**) and magnetic susceptibility (**b**) plots for the G–A section basalts. Note the increasing density and susceptibility with decreasing Mg #. Phenocryst-corrected densities are plotted in the figure. Schematic illustration of density variation during differentiation of a primitive basaltic magma (Sparks and Huppert 1984) is shown in the inset. The G–A section basalts record the A-B fractionation interval of the basalt differentiation path. Symbols as in Fig. 4

Fluid-dynamic models (Sparks and Huppert 1984) indicate that during fractionation of basaltic magma, density increases from the plagioclase-in stage (A in Fig. 5a inset) to the ilmenite- and/or magnetite-in stage (B in Fig. 5a inset). Density variation during the complete fractionation history of a Mg-rich basaltic parental magma (Sparks and Huppert 1984) is shown in the inset of Fig. 5. Decrease in liquid density from P to A is related to fractionation of olivine + spinel ± clinopyroxene in the early stages of primary basalt fractionation. Plagioclase and augite fractionation that records the interval between A and B increases the residual liquid density due to iron enrichment. Both petrographic and geochemical evidence provide support for the fractionation of plagioclase and clinopyroxene in the investigated rocks.

Magnetic susceptibility shows a vague negative correlation with Mg # (Fig. 5b). Magnetic susceptibility in the basaltic rocks is mainly controlled by the modal proportion of iron oxide minerals. Buldhana basalts with high modal ilmenite and magnetite expectedly show high magnetic susceptibility values. For reasons not yet resolved, some of the Karanja samples and all of the Ajanta samples record higher susceptibility for comparable Mg #s; at this juncture, we suspect that it could be due to low-temperature oxidation (maghemitisation) of ilmenite that is believed to increase the susceptibility of the rocks (Horen and Fleutelot 1998).

Both density and magnetic susceptibility track with the geochemical indicators, and act as proxies of magmatic processes. Increases in density and susceptibility during the fractionation of tholeiitic magma are strongly controlled by fO_2 conditions. During the differentiation of tholeiitic magma, values of fO_2 are very low during the initial stages; as a result, iron oxides do not crystallize and instead, iron is enriched in the residual liquids (Osborn 1959), thus increasing both density and magnetic susceptibility.

Pressure and temperature of fractional crystallization

Earlier studies have suggested that the fractionation and mixing of Deccan basaltic magmas operated in shallow crustal magma chambers (Aoki et al. 1992; Cohen and Sen 1994). Sano et al. (2001) further indicated that major element evolutionary trends depicted by the Deccan basalts are reproducible by fractionating the parental magma at atmospheric pressure and temperatures of the range 1120–1150°C.

Petrography and restricted major element chemistry suggest that the G–A section basalts are multi-saturated. This proposition can be evaluated by plotting the G–A

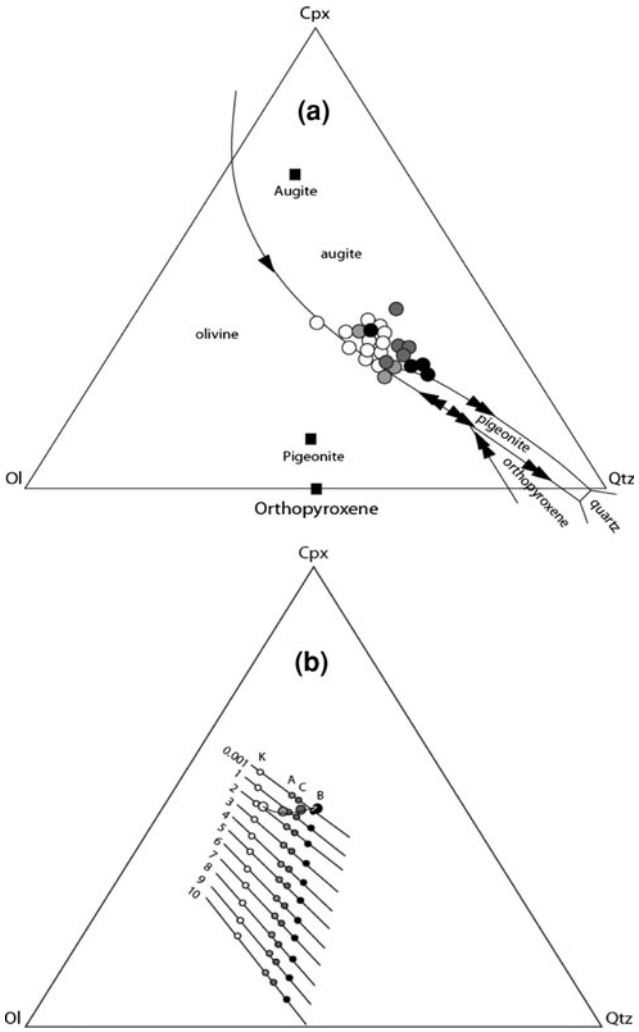

Fig. 6 Projection of plagioclase-saturated liquids in oxygen units from Pl + Or + Ilm components onto Ol–Di–Qtz phase equilibrium (**a**; after Grove 1993). Many of the G–A section basalts plot close to the Ol + Pl + Pig + Aug + Liq pseudo-invariant point, which is an olivine peritectic. *Single arrow* shows direction of decreasing temperature and *double arrow* indicates a reaction boundary. Calculated projection points (small symbols) of olivine–plagioclase–augite saturated liquids having the compositions of the average Ajanta (*A*), Chikhli (*C*) and Buldhana (*B*) formations of the G–A section [(Karanja (*K*) is represented by primitive sample 26)] for pressures ranging from 0.001 to 10 kbar using equations of Yang et al. (1996) plotted in the plagioclase-saturated pseudo-ternary olivine–clinopyroxene–quartz diagram using normative oxygen unit components (**b**; Grove 1993). Actual compositions of rocks are shown in bigger symbols. Presumed fractionation path from Karanja to Buldhana is shown

section basalts in plagioclase-saturated olivine-clinopyroxene-quartz pseudo-ternary diagram following the projection scheme of Grove (1993). All the G–A section basalts tract parallel to the olivine-augite boundary but very close to the low-pressure pseudo-ternary invariant point ol–aug–pig (+plag) (Fig. 6a), with Karanja basalts showing less-evolved and Buldhana basalts more evolved compositions. Although the Chikhli and Buldhana basalts contain up to 15% of phenocrysts, they also plot near the pseudo-ternary invariant point, implying that their major element composition was controlled by 'liquid' components and not by phenocrysts.

Multiple saturation of G–A section basalts allows us to calculate the final equilibration pressures and temperatures using the formulations of Yang et al. (1996). The equations express the mole fractions of Al, Ca and Mg in ol–plag–aug saturated basaltic liquids as function of other major cation mole fractions and pressure (0.001–10 kbar). Using the mole fractions of Si, Fe, Ti, Na and K from a whole-rock analysis, the mole fractions of Al, Ca and Mg can be calculated for a given pressure. As the actual equilibration pressure is approached, the calculated and measured Al, Ca and Mg would converge. These calculated parameters are plotted in terms of normative oxygen components (Grove 1993) within the ol–aug–qtz pseudo-ternary system for basalts (Yang et al. 1996). Maximum pressure of final equilibrium for the G–A section basalts (recorded by Karanja) is ~2 kbar (~6 km below the surface; Fig. 6b); the Ajanta magma fractionated at ~1 kbar and the Chikhli and Buldhana basaltic liquids attained final equilibrium at almost atmospheric pressures.

Temperatures, calculated for the pressure range 0.001–2 kbar, vary from 1134 to 1180°C. We have also calculated the temperatures based on olivine-basalt equilibrium (Table 1; Ford et al. 1983) and they are 10–20°C lower than the liquidus temperatures calculated from Yang et al. (1996) formulations. The small difference between liquidus temperatures and olivine equilibration temperatures suggest that the melt may have started crystallization almost instantaneously when it was ponded in the shallow magma chamber. The present work supports the earlier studies that the second stage fractionation of Deccan basalts was operated at shallow depths (Aoki et al. 1992; Cohen and Sen 1994; Sato et al. 2001). Many studies have shown that final pressures of equilibrium of basaltic liquids in the CFB provinces were attained around 3.8 kbar (12.2 km, considered to represent depth of brittle/ductile transition in the crust; Philpotts 1998 and references therein). The contrasting pressures of final equilibration in the DVP and other CFB provinces need to be assessed in order to understand continental crustal structure and basement composition. Xenolithic data indicate that the Precambrian basement beneath Deccan basalts is highly heterogeneous (Ray et al. 2008); whether this heterogeneity played any role in shallow ponding and fractionation of Deccan magmas in general (Sen 2001) and G–A section basalt magmas in particular require further investigations.

Regional chemostratigraphic correlations

Chemostratigraphic correlation of formations is based on the assumption that the magma-type of a particular formation is geochemically unique and is not repeated in the course of a flood basalt province evolution, as the formation presumably has a time connotation and magma-type need not have one. An important implication of this assumption is that the dynamical changes in source composition and sequential magma chamber processes are reflected in the erupted magmas. In the Deccan Volcanic Province, the Mahabaleshwar area in the SW part is considered as the type stratigraphic section of the Deccan as a whole. Here the Deccan Group is divided into three subgroups: Kalsubai, Lonavala and Wai, which are further divided into different formations. Earlier workers have proposed that the basalt formations from the eastern DVP mainly exhibit Poladpur-type and Ambenali-type chemostratigraphy (Jay and Widdowson 2008 and references therein).

Although, the regional chemostratigraphic correlations may help in geochemical mapping of the province, it is also possible that individual formations may also have had distinctly different chemical evolutionary histories (Sheth and Melluso 2008; Sheth et al. 2009). Our present results (Fig. 7) suggest that the Ajanta, Chikhli and Buldhana formations of eastern DVP have affinities of the Poladpur unit within southwestern DVP. The Buldhana Formation is very similar to the contaminated upper Poladpur flows. The Karanja basalts are relatively primitive and least contaminated. These characteristics are very typical of the Ambenali-type basalts of Southwest DVP. Based on trace element signatures, we suggest that the Ajanta, Chikhli and Buldhana formations are correlated with the Poladpur, and the Karanja Formation is analogous to the Ambenali Formation.

Spatial/temporal variations

Studies of the semi-continuous extrusive sequence of basalts help us to unravel the changing conditions of melting and/or source compositions, and sequential magma chamber processes. Recognition of magma pulses and magma mixing through geochemical variations within erupted basalts is akin to understanding these processes through cryptic (chemical) layering in mafic layered complexes. Magma chambers record processes of fractionation, magma replenishment, mixing and steady-state dynamics. Steady-state conditions are reflected in more or less constant geochemistry and petrophysics of the erupted basalts.

From the Ajanta to the Buldhana formation, a continuous upward decrease in the major elements compatible with fractionating phases in a basaltic melt is apparent. This feature in addition to (a) very thin red bole separating the Ajanta, Chikhli and Buldhana formations, (b) the

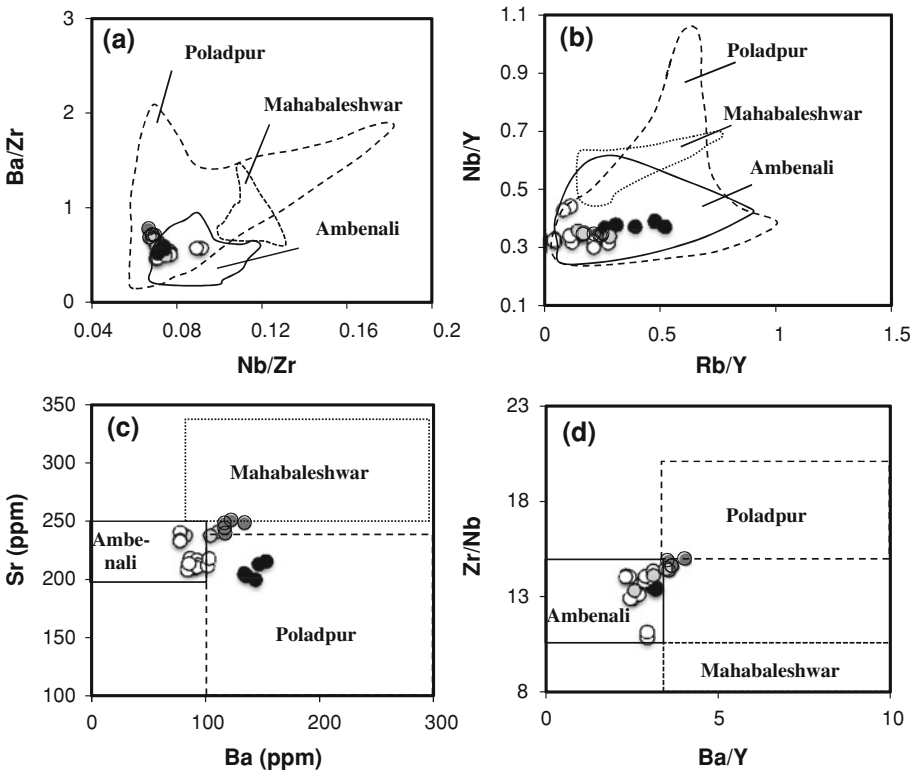

Fig. 7 Nb/Zr versus Ba/Zr (**a**), Rb/Y versus Nb/Y (**b**), Ba versus Sr (**c**) and Ba/Y versus Zr/Nb (**d**) plots for the G–A section basalts of the eastern DVP. Fields for Ambenali, Poladpur and Mahabaleshwar formations from the SWDVP are after Beane et al. (1986) and Devey and Lightfoot (1986). Note that eastern DVP basalts are geochemically similar to the Ambenali and Poladpur formations of the type area. Symbols as in Fig. 4

porphyritic nature of all three formations, (c) a concomitant increase in density and magnetic susceptibility, (d) a decrease in Ni, Cr and Sr contents, and (e) progressive increase in REE contents clearly indicates that these formations were derived from a single parental magma that underwent crystal fractionation in a magma chamber. These three formations represent semi-continuous eruptive pulses of residual liquid involving minor time gaps as indicated by the thin red boles. In contrast, the Buldhana–Karanja contact is signified by (a) a thick layer of red bole, (b) a sudden change in texture and mineral contents, (c) a decrease in density and magnetic susceptibility of the overlying Karanja unit, (d) an increase in MgO, CaO and Al_2O_3 contents, (e) an increase in Ni, Cr and Sr contents, (f) an increase in liquidus olivine temperature (calculated based on Ford et al. 1983 equation), and a drastic decrease in Rb and REE abundances and change in REE patterns. All of these features strongly suggest that basalts of the Karanja Formation represent a major magma addition to the magma chamber feeding the basalt pulses. Representative variations along the formational boundaries are shown in Fig. 8. Incompatible element ratios also shift marginally along the Buldhana–Karanja formational boundary (Fig. 8g, h, i). Our studies for the first time indicate that the Karanja Formation in the eastern DVP represents a zone of magma addition, distinct from the three lower units.

The geochemical variations documented in the G–A basalts with respect to stratigraphic position record three important magmatic processes. From the Ajanta to the Buldhana formations (360–460 m elevation), a steady decrease in MgO, and an increase in incompatible element concentrations, density and magnetic susceptibility reflect the process of fractional crystallization. In the overlying basalts (460–465 m elevation) abrupt increase in MgO contents, compatible element concentrations, and a drastic decrease in incompatible element concentrations, density and magnetic susceptibility are apparent. This is the stage when a major primitive melt may have replenished the magma chamber. Replenishment is critically reflected by abrupt geochemical and petrophysical variation with respect to stratigraphic horizon in the G–A basalts (Fig. 8). Addition of a new, less evolved liquid once again made the magma chamber dynamic, and a new cycle of fractional crystallization began. This major magma replenishment is recorded by the erupted Karanja basalts. A period of quiescence seems to have occurred between the major eruption of Karanja K1–K2 flows and the overlying flows. It is important to note that the K2 and K3 flows are separated by a $\sim$2 m red bole, and these quiescent intervals as represented by the red boles could be very short (Gérard et al. 2006). From the K3 flow upward, insignificant variation in chemistry and petrophysics reflects the attainment of a steady-state—the accumulating mineral phases were evidently in the same proportions as those that crystallized in the expelled liquid, thereby effecting only minor geochemical variations in the erupting basaltic liquid. Such a situation is possible only if the magma has reached the eutectic in a multicomponent system. This multiple saturation is characteristically shown by the G–A basalts (Fig. 6).

Discussion

In this section we discuss the geochemical variation recorded in G–A section basalts in terms of mantle and crustal processes. Crossing of the REE patterns among the G–A section volcanics and $(La/Nd)_N$ ratios less than unity in Karanja basalts suggest that simple melting and fractionation may not be responsible for these features. Different degrees of melting of a homogeneous source or different degrees of fractionation (accompanied by assimilation) from a single parental magma do not produce crossing REE patterns. It has been shown that dynamic melting of the mantle (Vijaya Kumar 2006; Vijaya Kumar et al. 2006 and references therein) and RTF processes within magma chambers (Elthon 1984) are capable of producing melts with crossing REE patterns and variable incompatible elemental ratios as measured in the analyzed G–A section basalts. Based on a detailed numerical experiment, Cox (1988) suggested that variations in inter-incompatible element ratios measured in a Deccan trap sequence cannot be explained by RTF processes with a constant composition for the replenishing magma. The existence of long-lived magma chambers, for the operation of RTF processes, was also ruled out in British Tertiary Volcanic Province (Skye plateau lavas; Dickin et al. 1984). It is possible that the crossing REE patterns for the melts originated in the mantle itself; in particular, the LREE-depleted Karanja basalts require a depleted mantle source. Further, the level of incompatible element enrichment in the Buldhana basalts cannot be explained by simple fractional crystallization; the involvement of upper continental crust is evident.

Parental magma and mantle source composition

Among the analyzed basalts, Karanja Formation sample 26, having the highest MgO, Ni and lowest Rb and REE concentrations, is the least differentiated. However, this sample does not represent the primary melt as its Mg # is only 0.6, and it also shows mild negative Eu anomalies. The primary mantle-derived magma would have Mg # 0.7 (BVSP 1981) and would lack any Eu anomalies, suggesting that 26 is fractionated. We have followed the method of

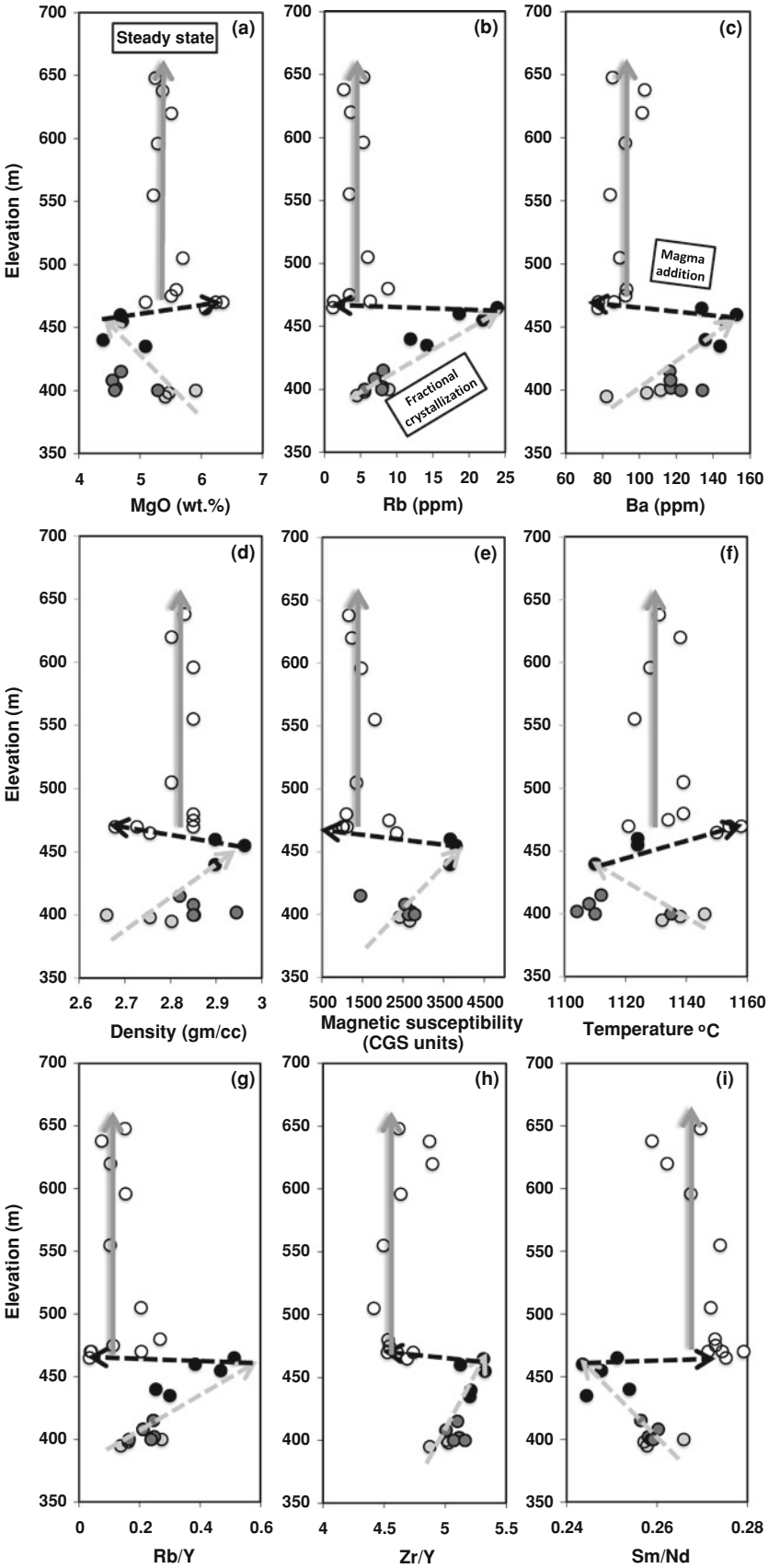

Fig. 8 Geochemical and petrophysical parameter variation with respect to elevation in the G–A section Deccan basalts. MgO (**a**) decreases with elevation up to 460 m then records a sudden increase with the beginning of Karanja Formation. From 500 m upwards, there is little variation in the MgO contents. Rb (**b**), Ba (**c**), density (**d**), magnetic susceptibility (**e**), increase and liquidus temperature (**f**) decrease with elevation up to 460 m, then show a drastic decrease/increase in the Karanja Formation, and again from 500 m upwards, all parameters show only minor variations. Minor variations in Rb/Y (**g**), Zr/Y (**h**) and Sm/Nd (**i**) are also recorded at the Buldhana–Karanja formational boundary. These variations in the erupted basalts are discussed in terms of magma addition, fractionation and steady-state within magma chamber, and are correspondingly labeled in the figure. Symbols as in Fig. 4

Hoffman and Feigenson (1983) for calculating the parental magma from the differentiated one. The method involves the addition of minerals that supposedly fractionated from the parental magma. The calculated REE pattern after removing the effects of the shallow fractionation (plagioclase) and deeper fractionation (olivine and clinopyroxene) is shown in the Fig. 9. Calculations are based on the Raleigh fractionation law (Neumann et al. 1954) using plagioclase, olivine and clinopyroxene mineral/melt partition coefficients (Bédard 2001).

The parental melt shows a convex-upward REE pattern, suggesting that the mantle source itself had a similar topology. The convex-upward REE pattern for the source possibly indicates two-stage melting of the mantle. In the first stage, low-degree melting of the originally LREE-enriched mantle would give rise to high $(La/Lu)_N$ alkaline magma (Fig. 9a). Separation of this high $(La/Lu)_N$ alkaline magma would make the source slightly depleted in LREE, and, as a result, it would form a convex-upward REE pattern. The REE pattern for the enriched mantle source shown in Fig. 9a is similar to that of the mantle source for continental-rift magmatism (see Vijaya Kumar and Rathna 2008 for details). Five percent continuous melting of the LREE-enriched source would produce a melt residue with convex-upward REE pattern after removing melt with higher $(La/Lu)_N$ ratios (Fig. 9a). The mantle residue thus formed is very similar to the calculated source for the Skye basalts (Wood 1979; Thompson et al. 1980), which are considered to have derived by polybaric mantle melting. The high $(La/Lu)_N$ alkaline melt thus produced in the first stage melting is very similar to the red bole (Fig. 9a). Could the red boles separating the formation boundaries represent low-degree melts derived from the mantle without modification in the magma chambers? Widdowson et al. (1997) suggested that some of the boles are different from basalts just above or below and may represent weathered pyroclastic material; the present study indicates that the original material could be alkaline in character.

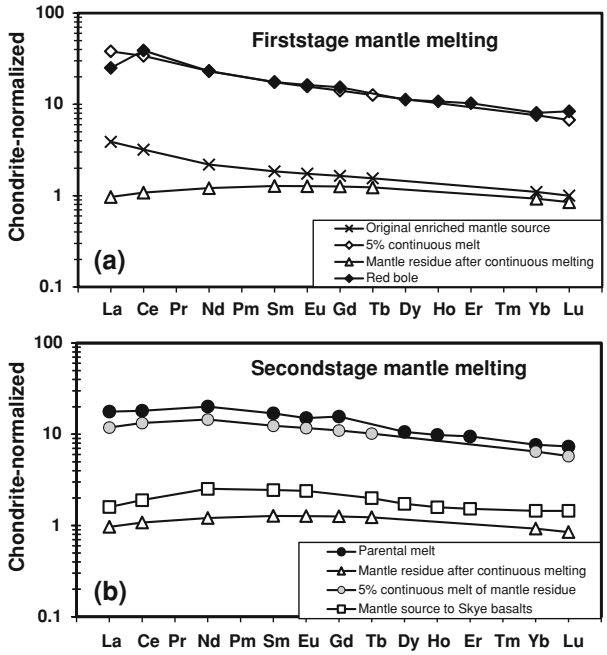

Fig. 9 Two-stage mantle melting model for the derivation of LREE-enriched and LREE-depleted basalts. (**a**) In the first stage, 4–5% melting of an enriched mantle (source for continental rift magmatism; Vijaya Kumar and Rathna 2008) produced high $(La/Lu)_N$ alkaline magma. The calculated melt pattern is very similar to the REE pattern of the red bole that separates the Buldhana and Karanja formations. Similarity of the calculated melt and red bole REE (except for La) suggests that most of the Ce peaks in Deccan weathered products, in reality, could be La troughs, and some of the red boles may represent low degree mantle melts. Removal of high $(La/Lu)_N$ melt by continuous melting of mantle produced mantle residue with convex-upward REE pattern. (**b**) In the second stage, 5–6% melting of the mantle residue (a total melting of 10–12%) produced the LREE-depleted melt parental to Karanja Formation. The parental melt to Karanja Formation was calculated by removing the effects of plagioclase, clinopyroxene and olivine fractionation from the least evolved basalt (sample 26). Mantle source for Skye basalts (Wood 1979) with convex-upward REE pattern is shown for comparison. A critical continuous melting equation (Sobolev and Shimizu 1992) was used in calculations; partition coefficients, and mantle source composition and melting proportions are after McKenzie and O'Nions (1991) and Shaw (2000), and Gurenko and Chaussidon (1995) respectively

In the second stage, the LREE-depleted source is further melted about 5% to produce melt with LREE-depleted signature that is compositionally similar to the parental melt to the Karanja Formation (Fig. 9b). It is well established that during formation of the Deccan basalts, the earliest episode produced alkaline magmas whereas later ones gave rise to tholeiitic basalts. Our model predicts that the tholeiitic basalts were derived from the residual mantle left after the removal of small pockets of alkaline melt. Such a model indicates that the Deccan mantle might have undergone dynamic melting to generate both LREE-enriched and -depleted basalts, and explains the REE crossings measured in the G–A section basalts. Modeling of mantle melting is based on critical continuous melting of Sobolev and Shimizu (1992) using published mantle mineral/melt partition coefficients (McKenzie and O'Nions 1991; Shaw 2000).

Magma chamber processes

Basalts of the Ajanta, Chikhli and Buldhana formations exhibit a gradual decrease in compatible element concentrations and an increase in incompatible element concentrations including REE, as generally expected in a progressively fractionating magma. But the Buldhana basalts show much higher Rb, REE and other *upper crustal* element abundances as compared to Chikhli basalts of

similar MgO contents. This suggests that Buldhana basalts might have undergone crustal contamination before attaining their present compositions. Modal orthopyroxene in Buldhana rocks may provide petrographic evidence for crustal contamination. It is well known that the interaction of basaltic magma with the granitic crust will crystallize orthopyroxene (Bowen 1928). In general the least contaminated Deccan basalts have higher TiO_2 (2–4 wt.%) and Sr (190–240 ppm) and lower Ba (<100 ppm) contents (Sano et al. 2001). But among the G–A section basalts Ti-rich Buldhana ($TiO_2 > 3$ wt.%) and Sr-rich Chikhli (~250 ppm) basalts record higher levels of crustal contamination (Ba = 116–153 ppm; Rb = 5–24 ppm).

Through a series of calculations using trace element concentrations, we have assessed the importance of assimilation-fractional crystallization (AFC) and crystal-laden melts in the geochemical variation of G–A section basalts (Fig. 10). Upper continental crust (Taylor and McLennan 1985) is considered as assimilate, and the ratio of the rate of assimilation to the rate of fractional crystallization (r) is considered as 0.2. Both fractional (Neumann et al. 1954) and assimilation fractional crystallization (DePaolo 1981) explain the measured Cr and Sr variation, but elevated concentrations of Sr in the Chikhli basalts are due to cumulus plagioclase. The importance of AFC and the cumulus nature of accessory minerals are brought out

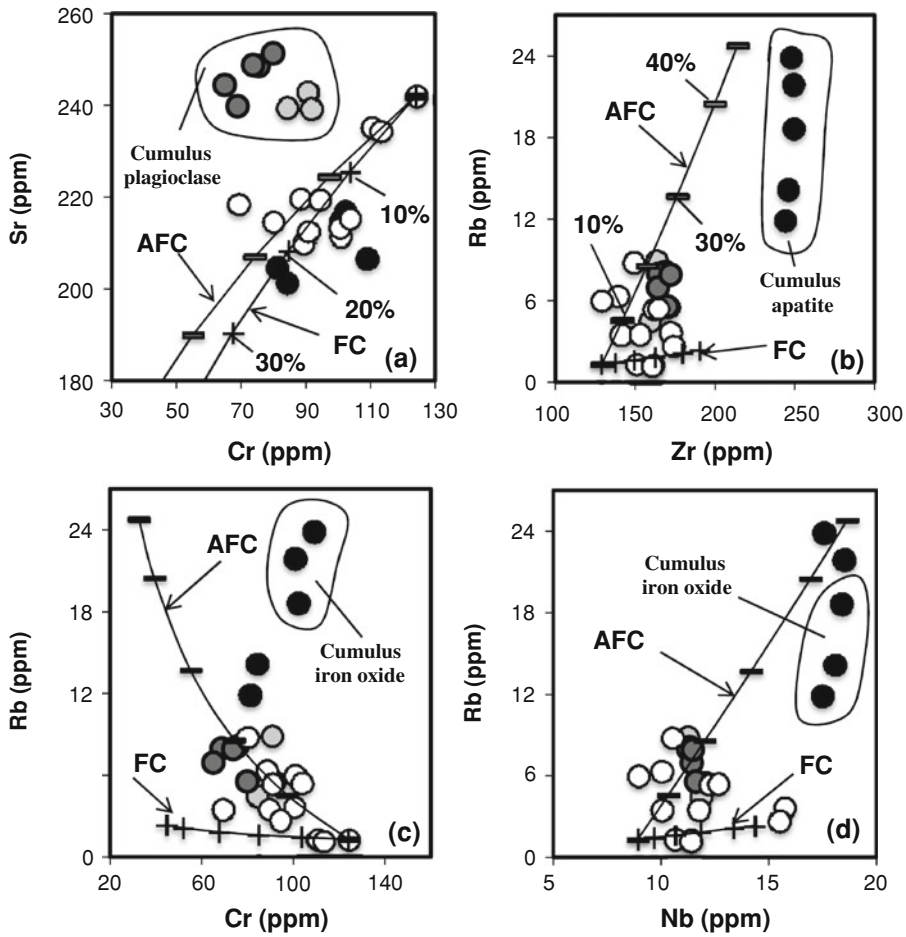

Fig. 10 Cr versus Sr (**a**), Zr versus Rb (**b**), Cr versus Rb (**c**) and Nb versus Rb (**d**) plots for the basalts of G–A section. Original compositions of the basalts are plotted to recognize cumulus phases especially in Chikhli and Buldhana formations. Liquid evolution curves were calculated for both fractional crystallization (FC) and assimilation fractional crystallization (AFC). Each tick on the fractionation curves indicates 10% fractionation (shown in **a** and **b**). Upper continental crust (Taylor and McLennan 1985) is used as assimilate. Ratio of the rate of assimilation to the rate of fractional crystallization (r) is considered as 0.2. Geochemical variation in the G–A section basalts is better explained by assimilation fractional crystallization. Note the deviations shown by Chikhli and Buldhana basalts from the calculated trends due to presence of cumulus phases. Symbols as in Fig. 4. Fractionation assemblage considered in the calculations is Pl = 50%, Cpx = 30%, Ol = 2%, Mt = 4%, Ilm = 4%, Ap = 1% and intercumulus liquid (ICL) = 9%. Equations for fractional crystallization and assimilation fractional crystallization are after Neumann et al. (1954) and DePaolo (1981) respectively; partition coefficients and upper continental crust assimilate composition are after Bédard (2001) and Taylor and McLennan (1985) respectively

by variation in Cr, Zr, Nb and Rb (Fig. 10). Although AFC calculations predict the observed Rb concentrations, the Buldhana basalts contain higher concentrations of Cr, Nb and Zr than predicted; cumulus ilmenite/magnetite and apatite can explain those concentrations as well as the elevated abundances of Ta, Y, and Hf. Cumulus plagioclase, oxide and apatite in the Chikhli and Buldhana basalts suggest that anorthosite and oxide–apatite-rich gabbros should be an integral part of the cumulate stratigraphy beneath the erupted basalts. If the order of fractionating mineralogy as revealed by textures and geochemical variation is any clue, the cumulate stratigraphy within shallow magma chambers beneath the erupted basalts should be olivine gabbro (troctolite) → leucogabbro (anorthosite) → oxide–apatite gabbro. The Phenai Mata complex, the only exposed shallow-level magma chamber in the Deccan Province, essentially contains the predicted layered sequence (Sukheswala and Sethna 1969; Prinzhofer et al. 1988).

Based on these observations, we have developed a model that summarizes the processes responsible for the petrographic, petrophysical and geochemical variation in the Deccan basalts in general, and the G–A section basalts in particular (Fig. 11). The model depicts dynamic melting of the mantle and two-stage differentiation of mantle-derived melts. Dynamic melting produces both LREE-enriched $[(La/Nd)_N > 1]$ and LREE-depleted $[(La/Nd)_N < 1]$ Mg-rich basaltic/picritic parental melts. The changing source composition from LREE-enriched to LREE-depleted with progressive melting is what constitutes the dynamic melting regime (Vijaya Kumar 2006 and references therein). The parental melts segregated within lower crustal magma chamber (s) and underwent the first stage fractional crystallization dominated by olivine and clinopyroxene (±spinel), thus producing Fe- and Al-rich tholeiitic melts (Fig. 11). Ni and Cr contents in the least evolved G–A section basalts suggest that they underwent extensive early, high-pressure fractionation of olivine and clinopyroxene. Fractionated melts migrated to upper crustal regions where the melts again ponded, but in shallow-level magma chambers. Second stage fractionation in these shallow magma chambers (~6 km depth) was dominated by plagioclase, olivine and clinopyroxene; oxide- and apatite-rich cumulates could also have been an integral part of these upper crustal cumulates. Trace element variation in the analyzed G–A section Deccan basalts is a reflection of the late, low-pressure fractionation. Our data indicates that fractionation was assisted by upper crustal contamination. Highly fractionated and contaminated melts erupt as continental flood basalts. Our model is similar to the

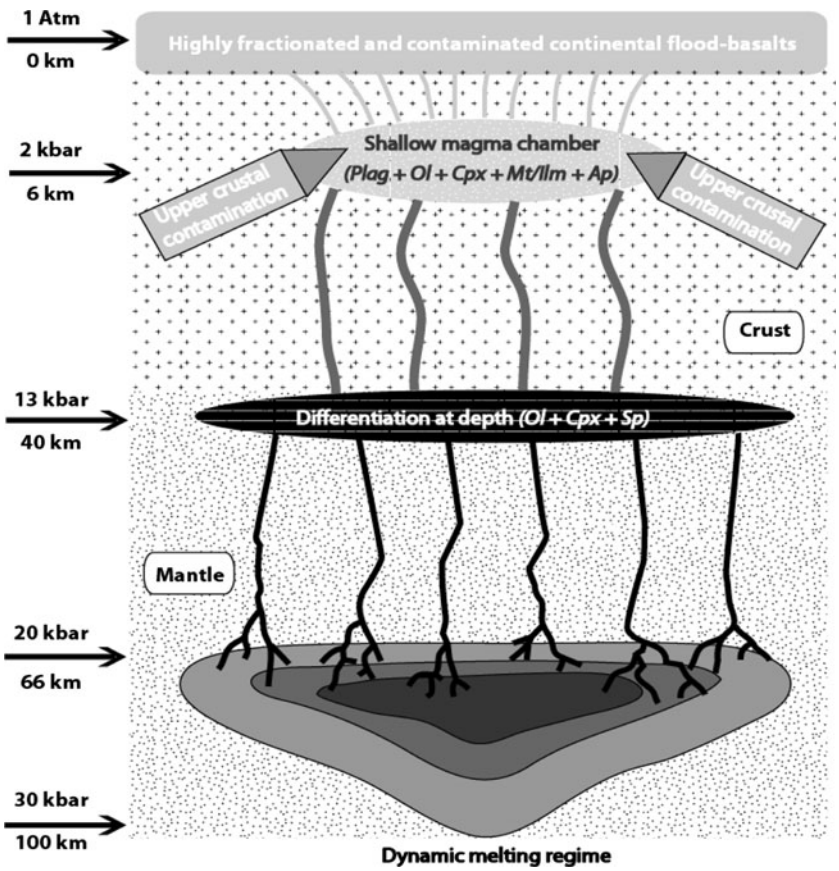

Fig. 11 A schematic model that summarizes the processes responsible for the petrographic, petrophysical and geochemical variation in the G–A section basalts. *Increasingly darker* shading in the dynamic melting regime represents increasingly melt-depleted portions. Two-stage fractionation accompanied by assimilation of mantle-derived dynamic partial melts explains the phase equilibria and geochemical characteristics of the Deccan basalts. Possible depths and pressures at which melting and crystallization processes operated are shown in the *left panel* of the diagram

classic paradigm for the continental flood basalt volcanism put forth by Cox (1980), but additionally illustrates the relevance of a dynamic melting regime, upper crustal contamination and apatite–oxide cumulates on the nature of erupted flood basalts.

Conclusions

We have conducted high-resolution chemical mapping of a 250 m thick, continuously exposed basaltic section of the eastern Deccan Volcanic Province, to understand mantle and magma chamber processes beneath flood basalt provinces. Dynamic melting of the mantle source, and magma chamber crystal fractionation, assimilation, addition of new magmas, and attainment of steady-state are recognized in the erupted basalts due to this high spatial resolution sampling.

The Ajanta, Chikhli, Buldhana and Karanja formations crop out in the area with increasing elevation. The erupted basalts underwent differentiation either on the surface or in shallow magma chambers at $\sim$6 km depth. Highly heterogeneous crust beneath the Deccan basalts, causing density heterogeneities, could be one of the factors for the ponding of the magma at these shallower depths. The predicted bottom-to-top sequence within the shallow magma chambers is olivine gabbro (troctolite) → leucogabbro (anorthosite) → oxide–apatite gabbro. The present study suggests that anorthosites and oxide–apatite-rich gabbros are an integral part of the cumulate stratigraphy beneath the mafic lavas. The Phenai Mata complex exhibits the predicted layered sequence (Sukheswala and Sethna 1969; Prinzhofer et al. 1988). The Ajanta, Chikhli and Buldhana basalts represent semi-continuous eruptive phases of an evolved liquid, reflecting brief time gaps. Geochemical variation in these three formations is due to assimilation-fractional crystallization of a single parental magma; Rb, Ba and REE concentrations indicate upper continental crust contamination within shallow magma chambers. The Karanja basalts record addition of a new magma pulse into this chamber. Replenishment of the shallow magma chamber is reflected by an abrupt change in textures, increase in MgO, CaO, Ni, Cr, and Sr, and decrease in Al_2O_3, Na_2O, K_2O, Rb, Ba, REE, and bulk-rock density and magnetic susceptibility along the Buldhana–Karanja boundary. Formational terminations in the Deccan basalts are generally correlated with the eruption of basalts containing giant plagioclase laths. Our present study shows that a small layer of oxide-rich basalts represents the latest erupted pulse in a given magmatic cycle. Due to higher density, its extrusive volume may be limited—hence this unit is easy to overlook in regional stratigraphic studies. Some of the red boles separating the formational boundaries may represent small degrees of melting of the mantle peridotite source that escaped magma chamber processes. In some cases, the well-known positive Ce anomalies in the red boles could be an artifact of La depletion.

Crossing of REE patterns in the erupted basalts reflect dynamic partial fusion of the mantle. Further, a convex-upward REE pattern for the (calculated) mantle source also suggests a two-stage mantle melting. Low degrees of melting in the first stage resulted in alkaline magmas, and partial fusion of the residues in the second stage produced tholeiitic basalts, as represented by the LREE-depleted Karanja samples. We suggest that dynamic melting of the mantle may be relevant to a fuller understanding of flood basalt geochemistry in general and Deccan geochemistry in particular. The present study illustrates the significance of detailed traverses across small stratigraphic intervals in unraveling complex mantle and magma chamber processes relevant to continental flood basalt volcanism.

Acknowledgments The manuscript has been reviewed and improved by Profs. C. Leelanandam, W.G. Ernst, A.R. Philpotts, C.J. Hawkesworth and official reviewers of the journal, Nilanjan Chatterjee and Loyc Vanderkluysen. T.L. Grove and A.R. Philpotts supplied the software for calculating phase equilibria projections and effect of pressure on the cotectic in multi-saturated systems and Chris Hawkesworth suggested including a model. The manuscript is an outcome of M.Sc. dissertation work carried-out in SRTM University. The first author's research at Stanford University is supported by the Indo-US Science and Technology Forum (IUSSTF) through a research fellowship. We gratefully acknowledge the above-named researchers and institutions for help.

References

Agarwal S, Bindal MM, Gupta AK (1990) High pressure-temperature studies on an olivine tholeiite and a tholeiitic picrite from the pavagarh region, Gujarat, India. Proc Indian Acad Sci (Earth Planet Sci) 99:91–98

Aoki K, Yoshida T, Aramaki S, Kurasawa H (1992) Low-pressure fractional crystallization origin of the tholeiitic basalts of the Deccan plateau, India. J Min Petrol Econ Geol 87:375–387

Basaltic Volcanism Study Project (BVSP) (1981) Basaltic Volcanism on the Terrestrial Planets. Pergamon Press, New York, p 1286

Beane JE, Turner CA, Hooper PR, Subbarao KV, Walsh JN (1986) Stratigraphy, composition and form of the Deccan basalts, Western Ghats, India. Bull Volcanol 48:61–83

Bédard JH (2001) Parental magmas of the Nain Plutonic Suite anorthosites and mafic cumulates: a trace element modelling approach. Contrib Mineral Petrol 141:747–771

Bhattacharji S, Sharma R, Chatterjee N (2004) Two- and three-dimensional gravity modeling along western continental margin and intraplate Narmada-Tapti rifts: its relevance to Deccan flood basalt volcanism. In: Sheth HC, Pande K (eds) Magmatism in India through time. Proc Indian Acad Sci (Earth Planet Sci) 113:771–784

Bilgrami SZ (1999) A reconnaissance geological map of the eastern part of the Deccan Traps (Bidar–Nagpur). In: Subbarao KV (ed) Deccan Volcanic Province. Geol Soc India Mem 43:219–232

Boudreau A, Philpotts AR (2002) Quantitative modeling of compaction in the Holyoke flood basalt flow, Hartford Basin, Connecticut. Contrib Mineral Petrol 144:176–184

Bowen NL (1928) The evolution of the igneous rocks. Princeton University Press, Princeton, p 332

Chakrabarti R, Basu AR (2006) Trace element and isotopic evidence for Archean basement in the Lonar crater impact breccias, Deccan Volcanic Provicne. Earth Planet Sci Lett 247:197–211

Chandrasekharam D, Mahoney JJ, Sheth HC, Duncan RA (1999) Elemental and Nd–Sr–Pb isotope geochemistry of flows and dikes from the Tapi rift, Deccan flood basalt province, India. J Volcanol Geotherm Res 93:111–123

Chandrasekharam D, Vaselli O, Sheth HC, Keshav S (2000) Petrogenetic significance of ferro-enstatite orthopyroxene in basaltic dikes from the Tapi rift, Deccan flood basalt province, India. Earth Planet Sci Lett 179:469–476

Chatterjee N, Bhattacharji S (2008) Trace element variations in Deccan basalts: roles of mantle melting, fractional crystallization and crustal assimilation. J Geol Soc India 71:171–188

Cohen TH, Sen G (1994) Fractionation and ascent of Deccan Trap magmas: an experimental study at 6 kilobar pressure. In: Subbarao KV (ed) Volcanism. Wiley Eastern, New Delhi, pp 173–186

Courtillot V, Davaille A, Besse J, Stock J (2003) Three distinct types of hotspots in the Earth's mantle. Earth Planet Sci Lett 205:295–308

Cox KG (1980) A model for flood basalt volcanism. J Petrol 21:629–650

Cox KG (1988) Numerical modelling of a randomised RTF magma chamber: a comparison with continental flood basalt sequences. J Petrol 29:681–697

Cox KG, Devey CW (1987) Fractionation processes in Deccan traps magmas: comments on the paper by G. Sen—Mineralogy and petrogenesis of the Deccan Trap lava flows around Mahabaleshwar, India. J Petrol 28:235–238

Cox KG, Hawkesworth CJ (1984) Relative contribution of crust and mantle to flood basalt magmatism, Mahabaleshwar area, Deccan traps. Phil Trans R Soc Lond A310:627–641

Cox KG, Hawkesworth CJ (1985) Geochemical stratigraphy of the Deccan traps at Mahabaleshwar, Western Ghats, India, with implications for open system magmatic processes. J Petrol 26:355–377

Cox KG, Mitchell C (1988) Importance of crystal settling in the differentiation of Deccan trap basaltic magmas. Nature 333:447–449

DePaolo DJ (1981) Trace element and isotopic effects of combined wallrock assimilation and fractional crystallization. Earth Planet Sci Lett 53:189–202

Dessai AG, Downes H, López-Moro F-J, López-Plaza M (2008) Lower crustal contamination of Deccan traps magmas: evidence from tholeiitic dykes and granulite xenoliths from western India. Mineral Petrol 93:243–272

Devey CW, Cox KG (1987) Relationships between crustal contamination and crystallization in continental flood basalt magmas, with special reference to the Deccan Traps of the Western Ghats, India. Earth Planet Sci Lett 84:59–68

Devey CW, Lightfoot PC (1986) Volcanological and tectonic control of stratigraphy and structure in the western Deccan traps. Bull Volcanol 48:195–207

Dickin AP, Brown JL, Thompson RN, Halliday AN, Morrison MA (1984) Crustal contamination and the granite problem in the British Tertiary volcanic province. Phil Trans R Soc Lond A310:755–780

Ellam RM, Cox KG (1991) An interpretation of Karoo picrite basalts in terms of interaction between asthenospheric magmas and the mantle lithosphere. Earth Planet Sci Lett 105:330–342

Ellam RM, Carlson RW, Shirey SB (1992) Evidence from Re-Os isotopes for plume-lithosphere mixing in Karoo flood basalt genesis. Nature 359:718–721

Elthon D (1984) Plagioclase buoyancy in oceanic basalts: chemical effects. Geochim Cosmochim Acta 48:753–768

Farnetani CG, Richards MN, Ghiorso MS (1996) Petrological models of magma evolution and deep crustal structure beneath hot spots and flood basalt provinces. Earth Planet Sci Lett 143:81–94

Fodor RV (1987) Low- and high-TiO_2 flood basalts of southern Brazil: origin from picritic parentage and a common mantle source. Earth Planet Sci Lett 84:423–430

Ford CE, Russel DG, Craven JA, Fisk MR (1983) Olivine-liquid equilibria: temperature, pressure and composition dependence of the crystal/liquid cation partition coefficients for Mg, Fe^{2+}, Ca and Mn. J Petrol 24:256–265

Fram MS, Lesher CE (1997) Generation and polybaric differentiation of east Greenland early Tertiary flood basalts. J Petrol 38:231–275

Furuyama K, Hari KR, Santosh M (2001) Crystallization history of primitive Deccan basalt from Pavagadh hill, Gujarat, Western India. Gondwana Res 4:427–436

Gérard M, Caquineau S, Chenet AL, Fluteau F, Courtillot V, Subbarao KV (2006) Red boles in the Deccan traps: time constraints from alteration processes. Geophys Res Abstracts 8:07092

Ghosh P, Sayeed MRG, Islam R, Hundekari SM (2006) Inter-basaltic clay (bole bed) horizons from Deccan traps of India: implications for palaeo-weathering and palaeo-climate during Deccan volcanism. Palaeogeo Palaeoclimat Palaeoeco 242:90–109

Gibson SA, Thompson RN, Dickin AP (2000) Ferropicrites: geochemical evidence for Fe-rich streaks in upwelling mantle plumes. Earth Planet Sci Lett 174:355–374

Grove TL (1993) Corrections to expressions for calculating mineral components in ''Origin of calc-alkaline series lavas at Medicine lake volcano by fractionation, assimilation and mixing'' and ''Experimental petrology of normal MORB near the Kane Fracture Zone: 22–25°N, mid-Atlantic ridge''. Contrib Mineral Petrol 114:422–424

Gurenko AA, Chaussidon M (1995) Enriched and depleted primitive melts in olivine from Icelandic tholeiites: origin by continuous melting of a single mantle column. Geochim Cosmochim Acta 59:2905–2917

Hanson GN (1980) Rare earth elements in petrogenetic studies of igneous systems. Annu Rev Earth Planet Sci 8:371–406

Hawkesworth CJ, Mantovani MSM, Peate DW (1988) Lithosphere remobilisation during Parana magmatism. In: Cox KG, Menzies MA (eds) Oceanic and Continental Lithosphere: similarities and differences. J Petrol Spec Issue, pp 205–223

Herzberg C, O'Hara (1998) Phase equilibria constraints on the origin of basalts, picrites and komatiites. Earth Sci Rev 44:39–79

Higgins MD, Chandrasekharam D (2007) Nature of sub-volcanic magma chambers, Deccan province, India: evidence from quantitative textural analysis of plagioclase megacrysts in the giant plagioclase basalts. J Petrol 48:885–900

Hoffman AW, Feigenson MD (1983) Case studies on the origin of basalt. I. Theory and reassessment of Grenada basalts. Contrib Mineral Petrol 84:382–389

Horen H, Fleutelot C (1998) Highly magnetized and differentiated basalts at the 18–19°S propagating spreading centre in the North Fiji Basin. Marine Geophy Res 20:129–137

Jay AE, Widdowson M (2008) Stratigraphy, structure and volcanology of the SE Deccan continental flood basalt province: implications for eruptive extent and volumes. J Geol Soc Lond 165:177–188

Jerram DW, Widdowson M (2005) The anatomy of Continental Flood Basalt Provinces: geological constraints on the processes and products of flood volcanism. Lithos 79:385–405

Jerram DA, Cheadle MJ, Philpotts AR (2003) Quantifying the building blocks of igneous rocks: are clustered crystal frameworks the foundation? J Petrol 44:2033–2051

Koroleva OV, Oleinikov BV, Zolotukhin VV (2002) Multiphase Phenai Mata intrusive complex (Deccan trap province, India) and its analogs on the Siberian platform. Russian Geol Geophys 43:916–927

Krishnamurthy P, Gopalan K, MacDougall JD (2000) Olivine compositions in picrite basalts and the Deccan volcanic cycle. J Petrol 41:1057–1069

Kumar S (2003) Variations in the thickness of the lithosphere underneath the Deccan volcanic province: evidence from rare earth elements. Mem Geol Soc India 52:179–194

Lightfoot PC, Hawkesworth CJ (1988) Origin of Deccan Trap lavas: evidence from combined trace element and Sr-, Nd- and Pb-isotope studies. Earth Planet Sci Lett 91:89–104

Lightfoot PC, Hawkesworth CJ, Devey CW, Rogers NW, van Calsteren PWC (1990) Source and differentiation of Deccan Trap lavas: implications of geochemical and mineral chemical variations. J Petrol 31:1165–1200

Mahoney J, MacDougall JD, Lugmair GW, Murali AV, Sankar Das M, Gopalan K (1982) Origin of the Deccan Trap flows at Mahabaleshwar inferred from Nd and Sr isotopic and chemical evidence. Earth Planet Sci Lett 60:47–60

Mahoney JJ, Sheth HC, Chandrasekharam D, Peng ZX (2000) Geochemistry of flood basalts of the Toranmal section, northern Deccan Traps, India: implications for regional Deccan stratigraphy. J Petrol 41:1099–1120

McKenzie D, O'Nions RK (1991) Partial melt distributions from inversion of rare earth element concentrations. J Petrol 32:1021–1091

Melluso L, Barbieri M, Beccaluva L (2004) Chemical evolution, petrogenesis, and regional chemical correlations of the flood basalt sequence in the central Deccan Traps, India. In: Sheth HC, Pande K (eds) Magmatism in India through Time. Proc Indian Acad Sci (Earth Planet Sci) 113:587–603

Melluso L, Mahoney JJ, Dallai L (2006) Mantle sources and crustal input as recorded in high-Mg Deccan traps basalts of Gujarat (India). Lithosphere 89:259–274

Mitchell CH, Widdowson M (1991) A geological map of the southern Deccan Traps, India and its structural implications. J Geol Soc Lond 148:495–505

Najafi SJ, Cox KG, Sukheswala RN (1981) Geology and geochemistry of the basalt flows (Deccan Traps) of the Mahad-Mahabaleshwar section, India. In: Subbarao KV, Sukheswala RN (eds), Deccan volcanism. Geol Soc India Mem 3:300–315

Neumann H, Mead J, Vitaliano CJ (1954) Trace element variation during crystallization as calculated from the distribution law. Geochim Cosmochim Acta 6:90–99

O'Hara MJ (1977) Geochemical evolution during fractional crystallization of a periodically refilled magma chamber. Nature 266:503–507

O'Hara MJ (2000) Flood basalts, basalt floods or topless Bushvelds? Lunar petrogenesis revisited. J Petrol 41:1545–1651

O'Hara MJ, Herzberg C (2002) Interpretation of trace element and isotope features of basalts: relevance of field relations, petrology, major element data, phase equilibria, and magma chamber modeling in basalt petrogenesis. Geochim Cosmochim Acta 66:2167–2191

O'Hara MJ, Mathews RE (1981) Geochemical evolution in an advancing, periodically replenished, periodically tapped, continuously fractionated magma chamber. J Geol Soc London 138:237–277

Osborn EF (1959) Role of oxygen pressure in the crystallization and differentiation of basaltic magma. Am J Sci 257:609–647

Pande K (2002) Age and duration of the Deccan Traps, India: A review of radiometric and palaeomagnetic constraints. Proc Indian Acad Sci (Earth Planet sci) 111:115–123

Peng ZX, Mahoney JJ (1995) Drillhole lavas from the northwestern Deccan Traps, and the evolution of Réunion hotspot mantle. Earth Planet Sci Lett 134:169–185

Peng ZX, Mahoney JJ, Hooper PR, Harris C, Beane JE (1994) A role for lower continental crust in flood basalt genesis? Isotopic and incompatible element study of the lower six formations of the western Deccan Traps. Geochim Cosmochim Acta 58:267–288

Peng ZX, Mahoney JJ, Hooper PR, MacDougall JD, Krishnamurthy P (1998) Basalts of the northeastern Deccan Traps, India: isotopic and elemental geochemistry and relation to southwestern Deccan stratigraphy. J Geophys Res 103:29843–29865

Philpotts AR (1998) Nature of a flood-basalt-magma reservoir based on the compositional variation in a single flood-basalt flow and its feeder dike in the Mesozoic Hartford Basin, Connecticut. Contrib Mineral Petrol 133:69–82

Philpotts AR, Dickson LD (2000) The formation of plagioclase chains during convective transfer in basaltic magma. Nature 406:59–61

Philpotts AR, Dickson LD (2002) Millimeter-scale modal layering and the nature of the upper solidification zone in thick flood-basalt flows and other sheets of magma. J Struct Geol 24:1171–1177

Philpotts AR, Shi J, Brustman C (1998) Role of plagioclase crystal chains in the differentiation of partly crystallized basaltic magma. Nature 395:343–346

Philpotts AR, Brustman C, Shi J, Carlson WD, Denison C (1999) Plagioclase-chain networks in slowly cooled basaltic magma. Am Mineral 84:819–1829

Prinzhofer A, Allegre CJ, Gwalani LG, Nicolas A (1988) Magma chamber in the Deccan traps (India). EOS 69:521

Raja Rao CS, Sahasrabudhe YS, Deshmukh SS, Raman R (1978) Distribution, structure and petrography of the Deccan Trap, India. Report Geol Survey India, 43 pp

Ray R, Shukla AD, Sheth HC, Ray JS, Duraiswami RA, Vanderkluysen L, Rautela CM, Mallik J (2008) Highly heterogeneous Precambrian basement under the central Deccan traps, India: direct evidence from xenoliths in dykes. Gondwana Res 13:375–385

Sano T, Fujii T, Deshmukh SS, Fukuoka T, Aramaki S (2001) Differentiation processes of Deccan trap basalts: contribution from geochemistry and experimental petrology. J Petrol 42:2175–2195

Sen G (1986) Mineralogy and petrogenesis of the Deccan trap lava flows around Mahabaleshwar, India. J Petrol 27:627–663

Sen G (2001) Generation of Deccan Trap magmas. Proc Indian Acad Sci (Earth Planet Sci) 110:409–431

Shaw DM (2000) Continuous (dynamic) melting theory revisited. Can Mineral 38:1041–1063

Sheth HC (2005a) From Deccan to Réunion: no trace of a mantle plume. In: Foulger GR, Natland JH, Presnall DC, Anderson DL (eds) Plates, plumes, and paradigms: Boulder, Colorado, Geol Soc Amer Spec Paper 388:477–501

Sheth HC (2005b) Were the Deccan flood basalts derived in part from ancient oceanic crust within the Indian continental lithosphere? Gondwana Res 8:109–127

Sheth HC, Melluso L (2008) The Mount Pavagadh volcanic suite, Deccan Traps: geochemical stratigraphy and magmatic evolution. J Asian Earth Sci 32:5–21

Sheth HC, Mahoney JJ, Chandrasekharam D (2004) Geochemical stratigraphy of flood basalts of the Bijasan Ghat section, Satpura Range, India. J Asian Earth Sci 23:127–139

Sheth H, Ray JS, Ray R, Vanderkluysen L, Mahoney JJ, Kumar A, Shukla AD, Das P, Adhikari S, Jana B (2009) Geology and geochemistry of Pachmarhi dykes and sills, Satpura Gondwana

Basin, central India: problems of dyke-sill-flow correlations in the Deccan Traps. Contrib Mineral Petrol 158:357–380
Shrivastava JP, Pattanayak SK (2002) Basalts of the Eastern Deccan volcanic province, India. Gondwana Res 5:649–665
Shukla AD, Bhandari N, Kusumgar S, Shukla PN, Ghevariya ZG, Gopalan K, Balaram V (2001) Geochemistry and magnetostratigraphy of Deccan flows at Anjar, Kutch. Proc Indian Acad Sci (Earth Planet Sci) 110:111–132
Sobolev AV, Shimizu N (1992) Ultra-depleted melts and permeability of the oceanic mantle (in Russian). Dokl Acad Sci Russia 236:354–360
Sparks RSJ, Huppert HE (1984) Density changes during the fractional crystallization of basaltic magmas: fluid dynamic implications. Contrib Mineral Petrol 85:300–309
Sparks RSJ, Meyer P, Sigurdsson H (1980) Density variation amongst Mid-ocean ridge basalts: implications for magma mixing and the scarcity of primitive lavas. Earth Planet Sci Lett 46:419–430
Stolper E, Walker D (1980) Melt density and the average composition of basalt. Contrib Mineral Petrol 74:7–12
Subbarao KV, Hooper PR (1988) Reconnaissance map of the Deccan Basalt Group in the Western Ghats, India. In: Subbarao KV (ed) Deccan flood basalts. Geol Soc India Mem 10 (enclosure)
Subbarao KV, Bodas MS, Hooper PR, Walsh JN (1988) Petrogenesis of Jawhar and Igatpuri formations, western Deccan basalt province, India. In: Subbarao KV (ed) Deccan flood basalts. Geol Soc India Mem 10:253–280
Subbarao KV, Chandrasekharam D, Navaneethakrishnan P, Hooper PR (1994) Stratigraphy and structure of parts of the central Deccan basalt province: eruptive models. In: Subbarao KV (ed) Volcanism. Wiley Eastern, New Delhi, pp 321–332
Sukheswala RN, Sethna SF (1969) Layered gabbro of the igneous complex of Phenai Mata, Gujarat state. J Geol Soc India 10:177–187
Sun S-s, McDonough WF (1989) Chemical and isotopic systematics of oceanic basalts: implications for mantle composition and processes. In: Saunders AD, Norry MJ (eds) Magmatism in the ocean basins. Geol Soc Lond Spec Publ 42:313–345
Taylor SR, McLennan SM (1985) The continental crust: its composition and evolution. Blackwell, Oxford, p 312
Thompson RN, Gibson IL, Marriner GF, Mattey DP, Morrison MA (1980) Trace-element evidence of multistage mantle fusion and polybaric fractional crystallization in the Palaeocene lavas of Skye, NW Scotland. J Petrol 21:265–293
Vijaya Kumar K (2006) Mantle melting models: an overview. Deep Continental Stud India Newslett 16:2–10
Vijaya Kumar K, Rathna K (2008) Geochemistry of the mafic dykes in the Prakasam alkaline province of Eastern Ghats Belt, India: implications for the genesis of continental rift-zone magmatism. Lithosphere 104:306–326
Vijaya Kumar K, Narsimha Reddy M, Leelanandam C (2006) Dynamic melting of the Precambrian mantle: evidence from rare earth elements of the amphibolites from the Nellore-Khammam schist belt, South India. Contrib Mineral Petrol 152:243–256
Wadia DN (1975) Geology of India, 4th edn. Tata McGraw-Hill, New Delhi, p 508
Widdowson M, Walsh JN, Subbarao KV (1997) The geochemistry of Indian bole horizons: palaeoenvironmental implications of Deccan intravolcanic palaeosurfaces. In: Widdowson M (ed), Palaeosurfaces: recognition, reconstruction and palaeoenvironmental interpretation. Geol Soc Lond Spec Publ 120:269–281
Wood DA (1979) Dynamic partial melting: its application to the petrogenesis of basalts erupted in Iceland, the Faeroe Islands, the Isle of Skye (Scotland) and the Troodos Massif (Cyprus). Geochim Cosmochim Acta 43:1031–1046
Yang H-J, Kinzler RJ, Grove TL (1996) Experiments and models of anhydrous, basaltic olivine-plagioclase-augite saturated melts from 0.001 to 10 kbar. Contrib Mineral Petrol 124:1–18